

RESEARCH MEMORANDUM

FLIGHT INVESTIGATION AND THEORETICAL CALCULATIONS
OF THE FUSELAGE DEFORMATIONS OF A SWEEP-WING
BOMBER DURING PUSH-PULL MANEUVERS

By Alton P. Mayo

Langley Aeronautical Laboratory
Langley Field, Va.

**NATIONAL ADVISORY COMMITTEE
FOR AERONAUTICS
WASHINGTON**

March 29, 1957
Declassified September 13, 1957

NATIONAL ADVISORY COMMITTEE FOR AERONAUTICS

RESEARCH MEMORANDUM

FLIGHT INVESTIGATION AND THEORETICAL CALCULATIONS
OF THE FUSELAGE DEFORMATIONS OF A SWEEP-WING
BOMBER DURING PUSH-PULL MANEUVERS

By Alton P. Mayo

SUMMARY

The results of fuselage-deflection measurements at three stations on the fuselage of a swept-wing bomber (Boeing B-47A) during 12 push-pull maneuvers are presented in the form of coefficients expressing the fuselage deflection due to the normal-acceleration loads, the pitching angular-acceleration loads, the pitching angular-velocity loads, and the combined effect of the zero-lift loads, fuselage dead weight, and landing-gear reactions. Comparisons are made between the experimental deflection coefficients and those obtained from theoretical calculations. An outline of the procedures used to obtain the experimental and the theoretical coefficients is presented.

INTRODUCTION

The design of a flexible airplane requires not only the determination of various aerodynamic and inertia load distributions that would occur under specified flight conditions but also the associated structural deformations. The computations are not only lengthy but are subject to numerous assumptions and the end result is sometimes in doubt.

In order to secure an indication of the accuracy obtainable in each component of the calculations, as well as the accuracy of the end results, an extensive research program was undertaken in which a Boeing B-47A was used to obtain the pertinent experimental data.

In one phase of the research program, deflections of various surfaces were measured for the purpose of comparing the measured deflections with the computed values. Some of the results of this phase have been presented in references 1, 2, and 3, which give the deflection influence coefficients for the wing and an analysis of the wing deflections obtained in symmetrical flight and in rolling maneuvers.

The present report is concerned with the analysis of the fuselage deflections obtained under symmetrical flight conditions. These fuselage deflections were analyzed to obtain coefficients expressing the deflection due to the normal-acceleration loads, the pitching angular-acceleration loads, the pitching angular-velocity loads, and the combined effect of the zero-lift loads, fuselage dead weight, and landing-gear reactions. Comparisons are made between the experimentally determined deflections and those calculated theoretically. The procedures by which the flight data were analyzed for the various effects, and the methods used in the theoretical calculations are presented.

SYMBOLS

l	section load, lb/in.
n	normal load factor measured at airplane center of gravity
Z	fuselage deflection measured from ground-zero position, positive downward, in.
Z'	fuselage deflection measured from no-load position, positive downward, in.
q	airplane pitching velocity, positive for nose pitching up, radians/sec
\dot{q}	airplane pitching acceleration, positive for increasing positive velocity, radians/sec ²
S_Z	standard error of estimate of equation for Z , in.

Subscripts:

n	derivative with respect to n for complete airplane
\dot{q}	derivative with respect to \dot{q} for complete airplane
q	derivative with respect to q for complete airplane
o	zero lift
i	combined landing-gear and dead-weight effects

Matrix:

$\left\{ \right\}$ column matrix

AIRPLANE AND TESTS

The airplane used in the test was a Boeing B-47A airplane. (See figs. 1 and 2.) The changes in the test airplane configuration from the standard airplane were the installation of an airspeed-measuring boom and fairing on the nose and an external canopy, housing the deflection-recording instruments, mounted atop the fuselage approximately at the intersection of the airplane center line and the wing 38-percent-chord line.

The flight-test data used in this paper pertain to push-pull maneuvers flown during the B-47A flight-research program conducted at the NACA High-Speed Flight Station at Edwards, Calif.

The push-pull maneuvers were made at altitudes of 25,000 and 30,000 feet with Mach numbers ranging from 0.51 to 0.80. The maneuvers in the present report were made with airplane gross weights of approximately 109,000 and 125,000 pounds and center-of-gravity positions of 13 percent and 22 percent mean aerodynamic chord. The normal load factor ranged from 0.3g to 1.5g and the pitching acceleration ranged from 0.16 to -0.14 radian per second per second. The specific values of Mach number, altitude, airplane weight, center-of-gravity position, dynamic pressure, and the weight of fuel in each fuel tank are given in table I for each run analyzed in this report. These are some of the runs for which the wing deflections were analyzed in reference 2.

INSTRUMENTATION AND ACCURACY OF MEASUREMENT

The instrumentation pertinent to this paper consisted of a pitch turnmeter, roll turnmeter, altimeter, airspeed indicator, normal accelerometer, aileron-position recorder, and an optigraph system for measuring the fuselage deflections. The roll turnmeter and the aileron-position recorder were used only to insure that the data selected were from push-pull maneuvers with little or no roll. The accelerometer was located at 34.25 percent mean aerodynamic chord, and the pitch turnmeter was located at 27.19 percent mean aerodynamic chord. Corrections were made to the normal-accelerometer data for the small displacements of the instrument from the airplane center of gravity. All instruments were of the standard NACA photographically recording type with the exception of the optigraph system which was designed especially for the B-47A airplane.

The fuselage optigraph system consisted of three target lamps on the fuselage and an optical recording instrument located atop the fuselage approximately at the intersection of the 38-percent-chord line of the wing and the center line of the fuselage. The recording instrument was a continuously recording camera mounted on a platform attached to

the wing carry-through section. (See fig. 3.) In order to facilitate the recording of the deflections with the optigraph in daylight, high-intensity infrared light sources were used in combination with infrared-sensitive recording film.

The optigraph system was calibrated through the use of a calibration stick with several infrared lamps spaced at 6-inch intervals and held vertically at each target station. All inflight measurements were made with reference to the fuselage-drooped position with the airplane resting on its landing gear.

The normal load factor and pitching angular-velocity values are estimated to be accurate to ± 0.01 and ± 0.005 radian per second, respectively. The pitching angular-acceleration values were obtained from measurements of the slopes of the pitching-velocity trace and are estimated to be accurate to ± 0.01 radian per second per second. The airplane weights listed in table I apply at the time of the maneuver and are estimated to be accurate to ± 500 pounds. The fuel weights for each tank are estimated to be accurate to ± 500 pounds per tank. The deflections are estimated to be accurate to ± 0.15 -inch incremental and ± 0.4 inch from ground-zero position.

METHOD AND RESULTS

In a symmetrical maneuver, the final fuselage-load distribution can be considered as resulting from the superposition of various types of load distributions. The fuselage structural deflections are assumed to be linearly related to these component loadings. In the analysis of the present paper, the final loading on the fuselage is considered to be composed of six components as follows:

- (1) A load distribution due to the fuselage angle of attack
- (2) A load distribution due to the wing-wash effects
- (3) A load distribution due to the loads induced by the wing
- (4) A load distribution due to the fuselage inertia loads (including horizontal and vertical tail)
- (5) A concentrated load at the $\bar{c}/4$ of the horizontal tail due to the horizontal-tail aerodynamic loads
- (6) A concentrated load at the wing-attachment pins due to the wing aerodynamic and inertia loads

Analysis of the Flight Data

In order to illustrate the type of data used in the analysis, typical time histories of the target deflections and the associated airplane motions are shown in figure 4. The variation of the fuselage deflection with normal load factor is shown in figure 5.

The procedure, by which such measurements were reduced to coefficients expressing the deflection of a point due to the various types of loads, makes use of the assumption that the small wing torsion effects which vary nonlinearly with the wing loads may be considered negligible. Thus the loads on any station of the fuselage of the flexible airplane resulting from the inflight aerodynamic and inertia loadings is given by equation (A10) of appendix A as

$$l = l_0 + l_n n + l_{\dot{p}} \dot{p} + l_q q \quad (1)$$

Because the deflections at any point on the fuselage are linearly related to the loads, the corresponding equation for the deflections due to the inflight loadings is

$$Z' = Z_0 + Z_n n + Z_{\dot{q}} \dot{q} + Z_q q \quad (2)$$

The deflections as measured in flight were referenced to a ground-zero condition and therefore included the fuselage deflections due to fuselage dead weight, landing gear, and the wing dead weight. The measured fuselage deflections may be expressed as

$$Z = (Z_0 + Z_1) + Z_n n + Z_{\dot{q}} \dot{q} + Z_q q \quad (3)$$

At this point it is sufficient to note that each Z coefficient in equation (3) may involve all the six-component loads due to fuselage angle of attack, wing wash, tail-load effects, and so forth, enumerated previously. A more detailed interpretation of each Z coefficient is given in appendix A.

In the data analysis the combined Z_0 and Z_1 deflections were obtained as one coefficient ($Z_0 + Z_1$) which expresses the fuselage deflection change from the measuring reference position on the ground

to the zero-load-factor flight position in the air. These combined deflections are hereafter referred to as zero-lift-plus-droop deflections.

Although it is relatively difficult to obtain the coefficients of equation (3) from flight data under conditions where n , \dot{q} , or q are all varying, a least-squares method of data reduction was used in the present report to determine all of the coefficients simultaneously.

During the tests, Mach number, dynamic pressure, weight, and center-of-gravity position were effectively constant for each run. Thus, for each target in each run, the deflections at the various stations may be represented in matrix notation

$$\{Z\} = (Z_0 + Z_1)\{1\} + Z_n\{n\} + Z_{\dot{q}}\{\dot{q}\} + Z_q\{q\}$$

where the columns $\{ \}$ are corresponding values of Z , n , \dot{q} , and q read from the flight records at 0.2-second time intervals during the run. The coefficients $(Z_0 + Z_1)$, Z_n , $Z_{\dot{q}}$, and Z_q were solved for by the method of least squares using approximately 25 data points per run. Least-squares procedure is described in detail in reference 3.

The values of the $(Z_0 + Z_1)$, Z_n , $Z_{\dot{q}}$, and Z_q coefficients obtained for each target in each run are presented in table II. Table III lists the coefficients, the standard errors of the coefficients, and the standard error of estimate S_Z , calculated by the method outlined in reference 3, for a typical run, that is, run 7 of flight 10. Typical fuselage-deflection curves formed by these coefficients are shown in figure 6. Plots of all the coefficients for each run are shown in figure 7. In order to illustrate the ability of the coefficients to predict the fuselage deflections, a comparison of the measured fuselage deflections with those determined by using equation (3) and the deflection coefficients is shown in figure 8 for flight 10, run 7.

Theoretical Calculations

In the calculations of the theoretical fuselage-deflection curves, the methods of reference 4 for the wing loads and wing wash were combined with the methods of references 5 and 6 for the loads induced on the fuselage by the wing and the loads due to fuselage angle of attack. The combination of these methods resulted in equations from which a simultaneous solution of all the aerodynamic loads on the airplane were determined. The procedure which was used is given in detail in appendix B.

The wing-structural stiffnesses used in the calculations were obtained from references 7 and 8. The fuselage structural stiffness was obtained from reference 9 with the exception of the fuselage section from station 742 to station 861 for which no data were available. The stiffness of this section was considered as an average of the section forward and rearward. The wing basic-weight distribution was obtained from reference 7 and was modified for the weight of the instrument installation. The fuselage-weight distribution was obtained from data on the XB-47 obtained from the manufacturer and was modified to include the weight of the instruments.

The theoretical wing-twist matrices required for the calculations were obtained by the methods of reference 4. The wing-deflection matrices were obtained from references 1 and 2. The downwash angles along the fuselage center line were calculated by the methods of reference 4, appendix E. The wing section lift-curve slopes were determined from the data of reference 10 by the method of reference 4 and corrected for Mach number effects by the Prandtl-Glauert equation.

Comparisons

Comparisons are shown in figures 9, 10, and 11 between the experimental and theoretical deflections due to the normal acceleration loads and the pitching-acceleration loads for two runs, one at a fairly high dynamic pressure and weight and one at a lower dynamic pressure and weight. The comparisons were restricted to two runs because the theoretical calculations were quite lengthy. Specifically, the comparisons made pertain to a Mach number of 0.60 at 25,000 feet, weight 108,700 pounds, and a Mach number of 0.76 at 30,000 feet and a weight of 125,400 pounds.

The comparisons between the calculated and the experimental deflections due to the normal acceleration loads are shown in figures 9 and 11. A complete solution, including all of the aerodynamic and inertia loads acting on the complete airplane and the theoretical deflections due to tail load and inertia effects only are shown. The deflections due to the tail load plus fuselage inertia were included in the figures to show that these effects are the major components of the fuselage deflections. The deflections due to the tail load plus fuselage inertia were obtained by using the theoretical tail load from the complete solution and the inertia loads, rearward of the front-spar attachment pin, were obtained from the fuselage-weight distribution. Details of the theoretical procedures are given in Appendix B. The experimental data points shown in the figures are plotted incrementally from a line through the deflection curve at fuselage stations 425 and 515.5 which is where the wing bay, on which the optigraph was mounted, is attached to the fuselage. In figure 9, the fuselage moment distribution is shown in order to illustrate

the shape of the distribution and the general magnitude of some of the components which combine to form the final moment distribution.

Similar comparisons for the fuselage deflections due to pitching acceleration are shown in figures 10 and 11. Again the moment distributions are included for illustrative purposes. The experimental data points are again plotted incrementally from a line through the theoretical curve at the wing-attachment stations.

DISCUSSION

Deflection Coefficients

Independent of any theoretical comparisons, the validity of the deflection coefficients obtained from the least-squares reduction of the flight data was substantiated by the facts that the coefficients:

- (1) Reestablished accurately the flight measurements from the measured airplane motions.
- (2) Established fuselage-deflection curves of expected shapes and magnitude due to the flight variables.
- (3) Showed erratic behaviors only when the deflections represented by the coefficient were approximately equal to the optigraph measuring accuracy.

The agreement shown in figure 8 between the measured fuselage deflections and the deflections calculated by using the deflection coefficients and the measured airplane motions indicates that equation (3) which was chosen to represent the data includes all of the important variables.

The shape of the deflection curve, formed by the $(Z_0 + Z_1)$ coefficients shown in figure 6, is believed to be due to the manner in which the fuselage bends between the landing gear and rear of the landing gear when the airplane is on the ground. Since this deflection curve involves several unknowns, it is difficult to establish its general shape, but it can be anticipated that the fuselage dead weight when combined with the landing-gear and wing dead-weight reactions would probably produce a fuselage-deflection curve with several inflection points. Examination of figure 7 in conjunction with table I shows that the $(Z_0 + Z_1)$ coefficients decrease with decreasing Mach number and dynamic pressure as could be expected from zero-lift considerations. Isolation of the various effects which are combined in the $(Z_0 + Z_1)$ coefficients was not possible because of the undetermined shape of the Z_1 deflection curve.

From theoretical considerations of the loads involved in the Z_n coefficients as shown in equation (A9) of Appendix A, it can be deduced that the Z_n coefficients vary with the weight of fuel in each tank, the dynamic pressure, and the Mach number. Several attempts were made to determine these independent variations but a sufficient amount and range of data were not available. However, examination of figure 7 in conjunction with the flight conditions of table I does show that the airplane with the heavier fuel weight produced the larger additional fuselage deflections. The Z_n deflections in every run were in the direction expected from considering only the inertia loads.

The Z_q coefficients also vary with Mach number, dynamic pressure, and fuel weight distribution. Unsuccessful attempts were made to determine the independent variations of the Z_q coefficients with these quantities, but sufficient data were not available. Examination of figure 7 in conjunction with the flight conditions of table I shows that the deflections due to pitching acceleration are largely affected by the amount of fuel in the tanks. The deflection variation from this component is, however, in the opposite direction expected from inertia considerations as the aerodynamic tail load associated with pitching acceleration is sufficiently large to overcome the inertia effects.

The Z_q coefficients are rather small and erratic and, as shown in table III, there are also fairly large standard errors for these coefficients. The inflight deflections resulting from pitching velocity would be only about 0.1 inch as predicted from the coefficients and the measured pitching velocity. Thus, the fuselage deflections due to pitching velocity are of about the same magnitude as the measuring accuracy of the optigraph system.

The experimental deflection coefficients were obtained with fuel conditions ranging from approximately 50-percent capacity to nearly full capacity. Within these weight limits, the Mach number and dynamic pressure at which the maneuvers were performed are sufficiently spread so that the incremental fuselage deflections could be closely predicted from the given coefficients for almost any longitudinal maneuver.

Theoretical Calculations and Comparisons

The flexibility of the fuselage between the wing carry-through bay attachment pins was considered in the theoretical fuselage-deflection calculations and this section of the fuselage had a high rate of curvature as is shown in figures 9, 10, and 11. Even though this fuselage section was considered flexible, the wing carry-through bay on which the optigraph was mounted was considered rigid and experienced a rotation

and translation as the attachment pins moved with fuselage bending. The optigraph was, therefore, assumed to be measuring from a rigid reference plane through the wing-bay attachment pins.

The effect of wing bending on the wing carry-through-bay deformations and thus on the optigraph measurements was also considered negligible. Calculations indicated that the maximum displacement of the carry-through bay at the airplane center line due to wing bending was approximately 0.15 inch for these maneuvers.

The assumption that the optigraph measured incremental values from the plane of the wing carry-through bay on which the optigraph (see fig. 3) was mounted is fairly accurate as evidenced by the agreement in figures 9, 10, and 11. In order to establish precisely the measurement reference line, the theoretical methods were set up to give deflection values at stations only 25 inches apart over the entire fuselage. The results were plotted to a scale 10 times as large as that of figures 9, 10, and 11 and the line was established and transferred to these figures.

The theoretical methods predicted the deflections due to the normal-acceleration loadings very well at the two conditions selected for comparisons; $M = 0.60$, weight = 108,700 pounds, and $M = 0.76$, weight = 125,400 pounds. From the bending-moment plot (fig. 9), it is evident that the normal-acceleration deflections are mainly an effect of inertia. The agreement shown between the deflections due to the tail load plus inertia and the deflections including fuselage airloads indicates that fuselage airloads have little effect on fuselage deflections. As previously mentioned, in calculating the deflections due to tail load plus inertia the effect of the inertia of the nose section was neglected, thus making the moment distribution zero at fuselage station 425 as shown in the figure.

The experimental and theoretical deflections due to pitching acceleration also showed very good agreement. In the case of pitching acceleration, as in the case of normal-acceleration effects, the deflections are due mainly to tail load plus inertia. In the case of pitching acceleration, however, the effect of the tail load exceeded the effect of inertia whereas in the case of the normal-acceleration deflections, the effect of tail load was small as compared to the effect of inertia.

No attempts were made to calculate the $(Z_0 + Z_i)$ coefficients due to the difficulty in determining the zero-lift loads and the ground-reaction forces at the various landing gears, nor were calculations made for the deflections due to pitching velocity because of the smallness of the measured deflections and the somewhat erratic behavior as indicated by the large standard errors.

In addition to the good agreements between experimental and theoretical deflections, the wing-root angle of attack, the tail load, and

the wing loads which were obtained directly from the theoretical solution also showed good agreement with the experimental data obtained from reference 11 and from preliminary results of strain-gage measurements on the wing and tail of the test airplane as obtained in the Flight Research Division of the Langley Aeronautical Laboratory as shown in table IV. The slight differences between the calculated center of gravity and the experimental value pertaining to the maneuver may be partly due to the fact that in the calculations the center of gravity of each section of the wing was assumed to be at the 38-percent-chord line.

The good agreement shown in the comparisons indicates that the fuselage deflections on this airplane may be calculated with a good degree of accuracy by existing methods from the known geometric structures and loadings.

CONCLUDING REMARKS

The inflight deflections of the fuselage have been analyzed by the method of least squares to obtain the component deflections due to the normal-acceleration loads, the pitching-acceleration loads, the pitching-velocity loads, and a combined loading due to the zero-lift loads, the fuselage dead-weight and landing-gear reactions. This type of analysis was validated by the consistency of the values obtained for the various coefficients and the ability of the coefficients to predict the fuselage deflections from the measured airplane motions.

The experimental data were obtained with fuel conditions ranging from approximately 50-percent capacity to full capacity. Within these weight limits the range in Mach number and dynamic pressure at which the maneuvers were performed is sufficiently large that the incremental fuselage deflections could be closely predicted for almost any longitudinal maneuver.

The comparison between the experimental fuselage deflections and those calculated with the fuselage weight and stiffness distributions by available aeroelastic methods indicates that adequate methods exist or can be devised for calculating the fuselage deflections on this airplane in quasi-static maneuvers.

The fuselage deflections on the airplane are mainly due to the effects of tail load and fuselage inertia. The inertia effect was the

major component of the deflections due to normal acceleration, whereas the tail-load effect was the larger component of the pitching-acceleration deflections.

Langley Aeronautical Laboratory,
National Advisory Committee for Aeronautics,
Langley Field, Va., November 16, 1956.

APPENDIX A

FUSELAGE DEFLECTION COEFFICIENTS

The fuselage loadings which are associated with the fuselage deflection coefficients are described in detail in this appendix. This detailed knowledge of the loads involved is also necessary in the calculation of the theoretical deflection coefficients for purposes of comparison.

Symbols Pertinent To Appendix A

m	airplane pitching moment, lb-in.
L	total load, lb
l	section load, lb/in.
n	normal load factor measured at airplane center of gravity
x_t	longitudinal distance from $\bar{c}/4$ of horizontal tail to airplane center of gravity, in.
Z'	fuselage deflection due to inflight loadings, positive downward, in.
q	airplane pitching velocity, positive for nose pitching up, radians/sec
\dot{q}	airplane pitching acceleration, positive for increasing positive velocity, radians/sec ²
W	weight of the airplane, lb
α	angle of attack, radians
α_r	wing-root incremental angle of attack (measured from the $n = 0$ position), radians

Differential operators:

$\frac{d}{d\alpha_{r,i=0}}$ variation with wing-root angle of attack for flexible airplane with no inertia forces acting

- $\frac{d\alpha_r}{dn}$ variation of wing-root angle of attack with normal load factor for complete airplane with aerodynamic and inertia forces acting ($q = \dot{q} = 0$)
- $\frac{dl}{dn_{i=0}}$ variation of load with normal load factor for flexible airplane with no inertia forces acting
- $\frac{d}{d_1 n}$ variation with normal load factor due to inertia loads plus aerodynamic loads caused by inertia deformations
- $\frac{d}{d_1 \dot{q}}$ variation with pitching acceleration due to \dot{q} inertia loads and aerodynamic loads caused by inertia deformations
- $\frac{d}{dq}$ variation with pitching velocity due to aerodynamic loads caused by pitching velocity (pitch axis for this case is station where α_r is defined)

Subscripts:

- n differential d/dn for the complete airplane
- \dot{q} differential $d/d\dot{q}$ for the complete airplane
- q differential d/dq for the complete airplane
- t pertaining to the tail
- f_l loads on the fuselage
- f fuselage
- o zero lift
- i inertia effects
- w wing
- a additional loads

Fuselage Load and Deflection Equations

The loads on the fuselage which cause the deflections are divided into the following main parts:

(1) The load imposed on the fuselage by the horizontal-tail aerodynamic loads. This load is considered concentrated at the $\bar{c}/4$ of the horizontal tail.

(2) The net load imposed on the fuselage by the wing, which is a result of the wing aerodynamic and inertia loads. This load includes the effects of wing wash, induced loads from the wing and the wing-attachment-pin loads.

(3) The load on the fuselage due to fuselage angle of attack combined with the fuselage loads due to its own inertia. The fuselage-inertia loads are considered to include the inertia load on both the horizontal and vertical tail.

These loads are a grouping of the fuselage loads enumerated in the section entitled "Method and Results." This loading breakdown may be expressed in equation form as

$$L_{\text{fuselage}} = L_{\text{fuselage due to tail}} + L_{\text{fuselage due to wing}} + L_{\text{fuselage due to fuselage}}$$

Each one of these three main loads is treated as a result of

- (1) The loads on the flexible airplane with no inertia forces acting.
- (2) The inertia loads combined with the aerodynamic loads resulting from the inertia deformations.

If the small variation in the center of pressure of the horizontal tail due to elevator deflection is neglected, then the aerodynamic tail load may be expressed by:

$$L_t = \left[m_{w+f,0} + \left(\frac{dm_{w+f}}{d\alpha_r, i=0} \right) \alpha_r + \left(\frac{dm_{w+f}}{d_1 n} \right) n + \left(\frac{dm_{w+f}}{d_1 \dot{q}} \right) \dot{q} + \left(\frac{dm_{w+f}}{dq} \right) q \right] + x_t \quad (A1)$$

These moments are about the airplane center of gravity. In this equation $\frac{dm_{w+f}}{d_1 n}$ is due solely to the aerodynamic loads arising from the inertia deformations since by definition of the center of gravity, the airplane inertia moment about the center of gravity due to load factor is equal to zero.

Thus the tail load may be expressed as

$$L_t = L_{t,0} + \left(\frac{dL_t}{d\alpha_{r,i=0}} \right) \alpha_r + \left(\frac{dL_t}{d_1 n} \right) n + \left(\frac{dL_t}{d_1 \dot{q}} \right) \dot{q} + \left(\frac{dL_t}{dq} \right) q \quad (A2)$$

It should be noted that $\frac{dL_t}{d_1 \dot{q}}$ is the aerodynamic tail load which balances the total airplane inertia moment and the aerodynamic effects resulting from the pitching-inertia deformations of the wing.

The load on the fuselage due to the fuselage-aerodynamic and inertia loads may be expressed by

$$l_{f,f} = l_{f,0} + \left(\frac{dl_f}{d\alpha_{r,i=0}} \right) \alpha_r + \left(\frac{dl_f}{d_1 n} \right) n + \left(\frac{dl_f}{d_1 \dot{q}} \right) \dot{q} + \left(\frac{dl_f}{dq} \right) q \quad (A3)$$

Also the loads on the wing are given by

$$l_w = l_{w,0} + \left(\frac{dl_w}{d\alpha_{r,i=0}} \right) \alpha_r + \left(\frac{dl_w}{d_1 n} \right) n + \left(\frac{dl_w}{d_1 \dot{q}} \right) \dot{q} + \left(\frac{dl_w}{dq} \right) q \quad (A4)$$

Since the loads on the fuselage due to the wing are linearly related to the wing loads, it follows that

$$l_{f,w} = l_{f,w,0} + \left(\frac{dl_{f,w}}{d\alpha_{r,i=0}} \right) \alpha_r + \left(\frac{dl_{f,w}}{d_1 n} \right) n + \left(\frac{dl_{f,w}}{d_1 \dot{q}} \right) \dot{q} + \left(\frac{dl_{f,w}}{dq} \right) q \quad (A5)$$

By considering the combined effects of equations (A2), (A3), and (A5), it can be seen that the load at any station on the fuselage may be expressed by

$$l = l_0 + \left(\frac{dl}{d\alpha_{r,i=0}} \right) \alpha_r + \left(\frac{dl}{d_1 n} \right) n + \left(\frac{dl}{d_1 \dot{q}} \right) \dot{q} + \left(\frac{dl}{dq} \right) q \quad (A6)$$

At all times during a maneuver the additional aerodynamic load on the airplane must balance the normal inertia forces plus any normal forces

resulting from the pitching-acceleration loads and the pitching-velocity loads so that

$$\left(\frac{dL_a}{d\alpha_r}\right)\alpha_r = nW + L\dot{q} + Lq \quad (A7)$$

where L_a is the normal resultant of all of the additional aerodynamic loads on the airplane. Dividing equation (A7) by W yields:

$$\left(\frac{dn}{d\alpha_r}\right)\alpha_r = n + \frac{L\dot{q}}{W} + \frac{Lq}{W}$$

where $\frac{dn}{d\alpha_r}$ is the variation of n with α_r for the airplane with \dot{q} and $q = 0$. Thus

$$\alpha_r = \left(n + \frac{Lq}{W} + \frac{L\dot{q}}{W}\right)\left(\frac{d\alpha_r}{dn}\right) \quad (A8)$$

Substituting equation (A8) into (A6) yields

$$\begin{aligned} l = l_0 + & \left[\left(\frac{dl}{dn_{i=0}}\right) + \left(\frac{dl}{d_1 n}\right) \right] n + \left[\left(\frac{dl}{dn_{i=0}}\right)\left(\frac{L\dot{q}}{W}\right) + \left(\frac{dl}{d_1 \dot{q}}\right) \right] \dot{q} + \\ & \left[\left(\frac{dl}{dn_{i=0}}\right)\left(\frac{Lq}{W}\right) + \left(\frac{dl}{dq}\right) \right] q \end{aligned} \quad (A9)$$

Each term of equation (A9) involves all of the component loads enumerated previously.

The term $\frac{dl}{dn_{i=0}}$ is defined as

$$\frac{dl}{dn_{i=0}} = \left(\frac{dl}{d\alpha_r, i=0}\right)\left(\frac{d\alpha_r}{dn}\right)$$

Thus the term $\frac{dl}{dn_i=0}$ is the variation with normal load factor of the additional fuselage load due to the flexible airplane with no inertia forces acting.

The loads on the fuselage are therefore expressible by

$$l = l_0 + l_n n + l_{\dot{q}} \dot{q} + l_q q \quad (\text{A10})$$

and since the deflections are linearly related to the loads:

$$Z' = Z_0 + Z_n n + Z_{\dot{q}} \dot{q} + Z_q q \quad (\text{A11})$$

APPENDIX B

OUTLINE OF THE METHODS USED TO OBTAIN THE
THEORETICAL DEFLECTION COEFFICIENTS

In the calculation of the theoretical deflections of the fuselage, the effects of the fuselage inertia loads, the fuselage aerodynamic loads, the tail load, and the forces at the wing-attachment pins must be considered. The final fuselage aerodynamic-load distribution is considered to be the sum of the components due to (1) the fuselage angle of attack, (2) the wing wash, and (3) the wing induction effects. Thus, it is evident that the wing, fuselage, and tail loads are interdependent; therefore, the solution for the fuselage loads due to normal acceleration must be obtained from an equilibrium equation which involves all of the airplane normal-acceleration loads. A similar procedure is required to determine the fuselage loads due to pitching acceleration.

The solution for the loads in the present case was obtained by a method somewhat similar to that of reference 4 which involves solving the wing load equations simultaneously with the total airplane force and moment equations which are expressed in terms of the wing loads, the fuselage loads, and the tail load. This solution yields directly the wing loads, the wing-root angle of attack, and the tail load. Using these knowns, all of the fuselage loads can be obtained.

Symbols Pertaining to Appendix B

A	fuselage cross-section area
a	maximum radius of fuselage
b	wing span
b_e	effective wing span for calculating wing-induced drag ($b_e = 0.9 \times b$ from ref. 12)
c	wing section streamwise chord measured at center of the section
\bar{c}	wing mean aerodynamic chord
$c_{d,0}$	wing section drag coefficient at $c_l = 0$
c_l	wing section lift coefficient

$$\left(C_{m\alpha,e}\right)_1 = dC_m/d\alpha \quad \text{for inboard nacelle}$$

$$\left(C_{m\alpha,e}\right)_2 = dC_m/d\alpha \quad \text{for outboard nacelle}$$

c_m	section pitching-moment coefficient
EI	fuselage structural stiffness, lb-in. ²
F	concentrated load, lb
h	semispan of bound leg of horseshoe vortex
H	height of plane of wing above fuselage center line
l_t	distance from $\bar{c}/4$ of horizontal tail to airplane center of gravity
L_t	tail load, lb
L_f	load on fuselage, lb
M	bending moment, lb-in.
m	airplane pitching moment, lb-in.
m_o	wing section lift-curve slope, per radian
q^*	dynamic pressure, lb/sq in.
S	wing area, sq in.
T_1	thrust of inboard nacelle, lb
T_2	thrust of outboard nacelle, lb
x	longitudinal ordinate
y	lateral ordinate (measured from and perpendicular to fuselage center line)
α_f	angle of attack of fuselage, radians
$\alpha_{i,1}$	streamwise angle of twist at inboard nacelle due to wing inertia, radians
$\alpha_{i,2}$	streamwise angle of twist at outboard nacelle due to wing inertia, radians

α_r	wing-root angle of attack, radians
$\alpha_{i,\dot{q}}$	wing twist due to $\dot{q} = 1$ inertia loads, radians
$\alpha_{i,n}$	wing twist due to $n = 1$ inertia loads, radians
α	angle of attack, radians
$\delta_{i,1}$	deflection of inboard nacelle due to inertia
$\delta_{i,2}$	deflection of outboard nacelle due to inertia

Matrix symbols:

$[A]$	structural matrix expressing wing angle of twist caused by nacelle pitching moment (see ref. 4)
$[D_E^o]$	deflections at center of wing sections due to combined wing aerodynamic and inertia loads at flight condition, in.
$[F_D^o]$	matrix of wing section drag, lb
$[2h^o]$	matrix of lengths of bound segment of wing horseshoe vortices
$[K_A^o]$	influence coefficient matrix expressing the wing deflection at inboard nacelle due to wing 0.25 chord airloads
$[K_B^o]$	influence coefficient matrix expressing wing deflection at outboard nacelle due to wing 0.25 chord airloads
$[K_I^o]$	matrix expressing induced loads on fuselage in terms of wing loads
$[K_\alpha^o]$	matrix expressing section loadings on fuselage in terms of fuselage section angle of attack
$[K_D]$	structural matrix expressing deflection of selected points on wing in terms of quarter-chord airloads
$[K_e^o]$	structural matrix expressing wing twist at inboard nacelle due to wing quarter-chord airloads

$\begin{bmatrix} \circ \\ K_f \end{bmatrix}$	structural matrix expressing wing twist at outboard nacelle due to wing quarter-chord airloads
$\{ l_w \}$	wing-section lift (including all flexibility effects), lb/in.
$\begin{bmatrix} \circ \\ L_w \end{bmatrix}$	load on wing panels of span $2h$, lb
$[S_1 + S_i]$	wing aerodynamic downwash matrix calculated from geometrical structure of wing and fuselage vortices
$[S_{1,D}]$	downwash matrix relating downwash at fuselage center line to wing loads
$[S_2]$	structural matrix expressing the wing streamwise twists due to wing quarter-chord airloads
$\begin{bmatrix} \circ \\ S_0 \end{bmatrix}$	fuselage overvelocity matrix expressing angle of attack on wing due to flow around fuselage (see ref. 4.)
$\begin{bmatrix} \circ \\ \Delta x \end{bmatrix}$	matrix of lengths of fuselage sections
$\{ \bar{x} \}$	moment arms to airplane center of gravity, in.
$\{ z_i \}$	deflection at selected points on wing due to wing and nacelle inertia
$\begin{bmatrix} \circ \\ 1.0 \end{bmatrix}$	diagonal matrix in which diagonal elements are equal to 1
$\{ \alpha_g \}$	wing section streamwise angle of attack in the flight condition as defined by equations (B20) and (B24)

Matrix notation:

$\{ \quad \}$	column matrix
$[\quad]$	square matrix
$\begin{bmatrix} \circ \\ \quad \end{bmatrix}$	diagonal matrix
$[\quad]$	row matrix

Subscripts:

l_w	wing quarter-chord airload
I_w	wing inertia
FS	wing front-spar attachment pin
RS	wing rear-spar attachment pin
nac	nacelles
w	wing
T	thrust of nacelles
t	tail
D	wing drag
L_c	chordwise component of wing section lift vector
f	fuselage

Fuselage Load Equations

Since the aerodynamic loads on the airplane in symmetrical maneuvers are symmetrical about the airplane center line, only one-half of the airplane will be considered in the equations to follow. The terms airplane moment and tail load and airplane inertia will refer to one-half of the airplane only.

The theoretical aerodynamic wing loads on one semispan are given by equation (24) of reference 4 as

$$\left[\begin{bmatrix} 1.0 & 0 \\ 0 & 1.0 \end{bmatrix} - q*S \begin{bmatrix} A \\ \end{bmatrix} \right] \begin{bmatrix} 0 \\ 1 \\ 4q*m_0 \end{bmatrix} \begin{bmatrix} S_1 + S_i \\ \end{bmatrix} - \begin{bmatrix} S_2 \\ \end{bmatrix} \left\{ l_w \right\} = \left\{ \alpha_g \right\} \quad (B1)$$

where $\left\{ \alpha_g \right\}$ includes the wing-root angle of attack, which was not included in the $\left\{ \alpha_g \right\}$ of reference 4. The geometric and downwash matrices of this equation were calculated for a vortex system of nine horseshoe vortices per semispan. The values of the section lift-curve slopes m_0 were determined through the use of equation (B1) as applied

to the wind-tunnel data of reference 10 and includes correction to the Mach number by the use of the Prandtl-Glauert equation. The required slopes of the nacelle pitching moment plotted against angle of attack were obtained from reference 12.

In the determination of the wing structural twist, the wing was treated as a cantilever fastened at the intersection of the fuselage wall and the wing 38-percent-chord line. The wing-bending and torsional-stiffness distributions of references 7 and 8 were used in the determination of the wing twist matrices. The influence coefficients of reference 1 were used to determine the deflection matrices.

For the fuselage load calculations, the fuselage was divided into seven segments forward and seven segments rearward of the wing root. The only loads considered on the fuselage in the section blanketed by the wing root were those induced from the wing.

The loads induced on each section of the fuselage by one wing semi-span may be deduced from equation (A4) of reference 5 as

$$\{L_f\} = \begin{bmatrix} 0 \\ K_I \end{bmatrix} \begin{bmatrix} 0 \\ 2h \end{bmatrix} \{L_w\} \quad (B2)$$

where the elements of $\begin{bmatrix} 0 \\ K_I \end{bmatrix}$ are expressed by

$$K_{i,j} = \frac{(y^2 - h^2 - H^2)a^2}{H^4 + 2H^2(y^2 + h^2) + (y^2 - h^2)^2}$$

The point of application of the fuselage loads is at the same longitudinal position as the section loads on the wing.

The loads on one-half the fuselage due to the fuselage angle of attack is given by equation (1) of reference 6 as

$$l = q \frac{dA}{dx} \sin \alpha$$

and for small angles of attack

$$l = q \frac{dA}{dx} \alpha$$

when the fuselage is considered in sections this expression becomes, for the part of the fuselage on one side of the fuselage center line

$$\{L_F\} = \begin{bmatrix} \overset{\circ}{\Delta x} \\ \overset{\circ}{K_\alpha} \end{bmatrix} \{1.0\} \alpha_F \quad (B3)$$

where for incremental angles $\alpha_F = \alpha_r$

The elements of $\begin{bmatrix} \overset{\circ}{K_\alpha} \end{bmatrix}$ are thus section values of $q \frac{dA}{dx}$. The section values of A were obtained by completing the fuselage-section drawings of reference 9 by consideration of the line drawings of the same reference and numerically integrating for the desired areas. The effect of the nose radar dome and canopy was neglected but small modifications were made for the angle-of-attack nose cone.

The load on each section of the fuselage due to wing wash from one semispan is given by

$$\{L_F\} = \begin{bmatrix} \overset{\circ}{\Delta x} \\ \overset{\circ}{K_\alpha} \end{bmatrix} \begin{bmatrix} \overset{\circ}{1} \\ \overset{\circ}{8\pi q^*} \end{bmatrix} \begin{bmatrix} S_{1,D} \end{bmatrix} \{l_w\} \quad (B4)$$

where $\begin{bmatrix} S_{1,D} \end{bmatrix}$ was calculated by the methods of reference 4, appendix E, and pertains only to one semispan.

The sum of the loads at the two wing-attachment pins due to the wing quarter-chord airloads is expressed by

$$L_{FS} + L_{RS} = [2h] \{l_w\} \quad (B5)$$

Airplane Pitching-Moment Component Equations

When the moment effects of the loads given by equations (B1) through (B5) are combined with the moments due to the nacelles and the moments due to the elevation of the line of action of the wing forces in the x-direction as caused by the wing deflections, the final airplane moment equations are established. The moments due to the fuselage loads are obtained by inserting the appropriate moment-arm matrices into the load equations.

Fuselage pitching-moment contributions.- The airplane moment due to the loads induced on the fuselage by one wing semispan is given from equation (B2) as:

$$\{m\} = \begin{bmatrix} \overset{\circ}{\bar{x}} \\ \overset{\circ}{K_I} \end{bmatrix} \begin{bmatrix} \overset{\circ}{2h} \end{bmatrix} \{l_w\} \quad (B6)$$

The airplane moment contribution of each fuselage section due to fuselage angle of attack is given from equation (B3) as

$$\{m\} = \begin{bmatrix} \overset{\circ}{\Delta x} \\ \overset{\circ}{K_\alpha} \end{bmatrix} \{\bar{x}\} \alpha_r \quad (B7)$$

where for incremental angles

$$\alpha_r = \alpha_f$$

The airplane moment contributed by each fuselage section due to wing wash of one semispan acting on the fuselage is given from equation (B4) as:

$$\{m\} = \begin{bmatrix} \overset{\circ}{\bar{x}} \\ \overset{\circ}{\Delta x} \\ \overset{\circ}{K_\alpha} \end{bmatrix} \begin{bmatrix} \overset{\circ}{1} \\ \overset{\circ}{8\pi q^*} \end{bmatrix} \begin{bmatrix} \overset{\circ}{S_{l,D}} \end{bmatrix} \{l_w\} \quad (B8)$$

Wing pitching-moment contributions.- The airplane moment due to the wing quarter-chord airload is given by

$$\{m\} = \begin{bmatrix} \overset{\circ}{\bar{x}} \\ \overset{\circ}{2h} \end{bmatrix} \{l_w\} \quad (B9)$$

The airplane moment due to the line of action of the chordwise component of wing section drag being elevated by the deflection of the wing is given approximately by

$$\{m\} = \begin{bmatrix} \overset{\circ}{F_D} \\ \overset{\circ}{K_D} \end{bmatrix} \{l_w\} + \begin{bmatrix} \overset{\circ}{F_D} \end{bmatrix} \{z_i\} \quad (B10)$$

where $\cos \alpha$ is assumed equal to 1 and

$$F_D = \left(c_{d,o} + \frac{c_l^2}{\pi b_e S} \right) q_2 h c$$

The airplane moment due to the line of action of the chordwise component of the lift vector being elevated by the deflection of the wing is given approximately by

$$\{m\} = \begin{bmatrix} \circ \\ L_w \end{bmatrix} \begin{bmatrix} \circ \\ D_E \end{bmatrix} \begin{bmatrix} \circ \\ S_2 \end{bmatrix} \{l_w\} - \begin{bmatrix} \circ \\ L_w \end{bmatrix} \begin{bmatrix} \circ \\ D_E \end{bmatrix} \{1.0\} \alpha_r - \begin{bmatrix} \circ \\ L_w \end{bmatrix} \begin{bmatrix} \circ \\ D_E \end{bmatrix} \{\alpha_1\} \quad (B11)$$

where $\sin \alpha$ is assumed equal to α and $\begin{bmatrix} \circ \\ S_2 \end{bmatrix} \{l_w\} + \{1.0\} \alpha_r + \{\alpha_1\}$ is the wing-section angle of attack.

Nacelle pitching-moment contribution. - The moment due to the nacelle-thrust line being elevated by the deflection of the wing as caused by the 0.25-chord airloads is given by

$$\{m\} = T_1 \begin{bmatrix} \circ \\ K_A \end{bmatrix} \{l_w\} + T_2 \begin{bmatrix} \circ \\ K_B \end{bmatrix} \{l_w\} \quad (B12)$$

The moment due to the nacelle-thrust line being changed by the inertia of the wing is given by

$$m = T_1 \delta_{i,1} + T_2 \delta_{i,2} \quad (B13)$$

The airplane moment due to the nacelle pitching moment caused by the wing twist resulting from the wing 0.25-chord airloads is given by

$$m = (C_{m_{\alpha,e}})_1 q^* S \bar{c} \begin{bmatrix} \circ \\ K_e \end{bmatrix} \{l_w\} + (C_{m_{\alpha,e}})_2 q^* S \bar{c} \begin{bmatrix} \circ \\ K_f \end{bmatrix} \{l_w\} \quad (B14)$$

The airplane moment resulting from the nacelle pitching moment due to wing-root angle of attack and wing inertia twist is given by

$$m = \left[(C_{m_{\alpha,e}})_1 + (C_{m_{\alpha,e}})_2 \right] (q^* S \bar{c} \alpha_r) + (C_{m_{\alpha,e}})_1 (q^* S \bar{c} \alpha_{1,1}) + (C_{m_{\alpha,e}})_2 (q^* S \bar{c} \alpha_{1,2}) \quad (B15)$$

Load Solutions

In equations (B10) and (B11), the terms $\begin{bmatrix} \circ \\ F_D \end{bmatrix}$, $\begin{bmatrix} \circ \\ D_E \end{bmatrix}$, and $\begin{bmatrix} \circ \\ L_W \end{bmatrix}$ occur. Since it is necessary to have all of the moment equations involve only the unknowns $\{l_w\}$ and α_r , a preliminary solution of equation (B1) must be made in order to obtain approximate values for $\begin{bmatrix} \circ \\ D_E \end{bmatrix}$, $\begin{bmatrix} \circ \\ F_D \end{bmatrix}$, and $\begin{bmatrix} \circ \\ L_W \end{bmatrix}$. This is accomplished by solving equation (B1) simultaneously with a preliminary normal-force equation and letting α_r and $\{l_w\}$ be the unknowns. In the preliminary normal-force equation, the loading inboard of the fuselage wall was assumed to be that of the most inboard wing section. Thus, preliminary force equation in matrix form was

$$[2h, 2h, 2h, \dots, 2h, 2h + 45] \{l\} = nw \quad \text{or} \quad L_{T,\dot{q},i}$$

Whether to use nw or $L_{T,\dot{q},i}$ depends on whether the solution is for normal-acceleration or pitching-acceleration loads. From these approximate wing loads, approximate wing deflections are determined by taking inertia effects into account. Thus, approximate $\begin{bmatrix} \circ \\ D_E \end{bmatrix}$ values are also obtained.

The moment contributions of equations (B10) and (B11) are small and could be neglected without appreciable error but were retained in the solutions of this paper as a matter of interest and solution refinement. If these equations were neglected, then the need for a preliminary solution would be eliminated since the purpose of the preliminary solution is to reduce equations (B10) and (B11) from second and third power expressions of the wing loads to an approximate linear form. Calculations show that these nonlinear effects do not appreciably affect the assumptions of linear variations of the loads at the wing-attachment pins as assumed in the data analysis of this report.

The solution of the preliminary equations provide excellent data to keep constant check on the final solution.

Equations (B13) and (B15) may be added to form the equation:

$$m = e\alpha_r + f \quad (\text{B16})$$

Also after values of $\begin{bmatrix} \circ \\ F_D \end{bmatrix}$ and $\begin{bmatrix} \circ \\ L_w \end{bmatrix}$ and $\begin{bmatrix} \circ \\ D_E \end{bmatrix}$ are established the remaining moment equations of (B6) to (B14) may be added to form the equation:

$$\{m\} = [q] \{l_w\} + \{h\} \alpha_r + \{j\} \quad (B17)$$

where each row of each matrix represents the moment contribution of a section of the fuselage or the wing. The elements of each column of equation (B17) may be added to form a moment equation

$$m = [P] \{l_w\} + B \alpha_r + G$$

to which equation (B16) may be added to form a moment equation of the same form

$$m = [Q] \{l_w\} + R \alpha_r + V$$

Also adding the tail contribution yields the total airplane aerodynamic-moment equation

$$m = [Q] \{l_w\} + R \alpha_r + V + L_t l_t \quad (B18)$$

Similar additions of the force equations will yield a similar equation

$$F = [\phi] \{l_w\} + w \alpha_r + L_t \quad (B19)$$

Solving equations (B1), (B18), and (B19) simultaneously will yield the wing loads, the tail load, and the wing-root angle of attack. The values of $\{\alpha_g\}$ and the summation of the moments and the forces must be prescribed for the flight condition for which the loads are to be determined.

Solution for the Fuselage Deflections Due to the
Normal Acceleration Loads

In the calculation of the deflection due to the normal-acceleration loads, the aerodynamic loads were obtained by solving simultaneously equations (B1), (B18), and (B19). The force equation was set equal to the $n = 1$ inertia load and the moment equation was set equal to zero. The values of $\{\alpha_g\}$ were given by

$$\{\alpha_g\}_{n=1} = \{\alpha_{i,n}\}(1.0) + \begin{bmatrix} 0 \\ S_0 \end{bmatrix} \{\alpha_r\} + \{1.0\}\alpha_r \quad (B20)$$

The simultaneous solution gives values of α_r , L_t , and l_w . With these knowns, the fuselage loads other than L_t and the attachment-pin reactions were obtained from equations (B2), (B3), and (B4). The loads at the attachment pins were determined from the solutions of the equations

$$\left. \begin{aligned} F_{FS}\bar{x} + F_{RS}\bar{x} &= m_{nac} + m_{l,w} + m_{i,w+nac} + m_D + m_{L,c} + m_T \\ F_{FS} + F_{RS} &= L_w + L_{i,w+nac} \end{aligned} \right\} \quad (B21)$$

The terms on the right-hand side of the equations can be obtained by using the previously established moment and load equations and the now known values of $\{l_w\}$ and $\{\alpha_r\}$.

The fuselage inertia loads were obtained from the dead-weight distribution. The distributions of fuselage weights, fuselage stiffness, and the variations of the fuel-tank centers of gravity with the amount of fuel are given in figures 12, 13, and 14, respectively. The fuel-tank centers of gravity were obtained from the data given in reference 13.

From the known fuselage aerodynamic and inertia loads, the bending moments were obtained by numerical integration of the equation

$$M_B = \iint l \, dx \, dx \quad (B22)$$

The deflections were obtained by the double numerical integration of the equation

$$Z' = \iint \frac{M}{EI} dx dx \quad (B23)$$

The fuselage weight and stiffness distributions were obtained from reference 9 and from data obtained from the manufacturer, being modified in the manner described in the text. The stiffness distribution used was for the B-47B airplane. The differences between the stiffnesses of the B-47A and B-47B fuselages are believed to be small.

Solution for the Deflections Due to Pitching Acceleration

In the calculation of the deflections due to pitching acceleration, the procedure was similar to that used for the normal-acceleration deflections. In this case the force equation was set equal to zero and the moment equation was set equal to the inertia moment. The values of

$\{\alpha_g\}$ were defined by

$$\{\alpha_g\}_{\dot{q}=1} = \{\alpha_{i,\dot{q}}\}(1.0) + [S_o^o]\{\alpha_r\} + \{1.0\}\alpha_r \quad (B24)$$

The fuselage inertia loads were obtained from the dead-weight distribution and consideration of the accelerations at the various fuselage sections.

REFERENCES

1. Mayo, Alton P., and Ward, John F.: Experimental Influence Coefficients for the Deflection of the Wing of a Full-Scale, Swept-Wing Bomber. NACA RM L53L23, 1954.
2. Mayo, Alton P., and Ward, John F.: Flight Investigation and Analysis of the Wing Deformations of a Swept-Wing Bomber During Push-Pull Maneuvers. NACA RM L54K24a, 1955.
3. Mayo, Alton P., and Ward, John F.: Flight Investigation and Analysis of the Wing Deformations on a Swept-Wing Bomber During Rolling Maneuvers. NACA RM L56C23a, 1956.
4. Gray, W. L., and Schenk, K. M.: A Method for Calculating the Subsonic Steady-State Loading on an Airplane With a Wing of Arbitrary Plan Form and Stiffness. NACA TN 3030, 1953.
5. Zlotnick, Martin, and Robinson, Samuel W., Jr.: A Simplified Mathematical Model for Calculating Aerodynamic Loading and Downwash for Wing-Fuselage Combinations With Wings of Arbitrary Plan Form. NACA TN 3057, 1954. (Supersedes NACA RM L52J27a.)
6. Weber, J., Kirby, D. A., and Kettle, D. J.: An Extension of Multhropp's Method of Calculating the Spanwise Loading of Wing-Fuselage Combinations. Rep. No. Aero 2446, British R.A.E., Nov. 1951.
7. Payne, Alan: Wing Stress Analysis. [Models XB-47 and B-47a.] Document No. D-7740 (Contract Nos. W33-038 ac-8429 and ac-22413), Boeing Airplane Co. Aug. 14, 1947.
8. Parsons, Cecil E.: Wing Destruction Tests - Model B-47B. Test No. T-25299 (Contract No. W33-038 ac 22413). Boeing Airplane Co. (revised Apr. 14, 1951).
9. Josendal, V.: Fuselage Stress Analysis. [Model B-47B.] Doc. No. D-10208 (Contract No. W33-038 ac-22413), Boeing Airplane Co., May 25, 1950 (revised Aug. 24, 1950).
10. Spangler, T. A.: The Span-Load Distribution of the XB-47 Wing. Doc. No. D-8055, Boeing Airplane Co., Dec. 24, 1946.
11. Aiken, William S., Jr., and Fisher, Raymond A.: Lift-Curve Slopes Determined in Flight on a Flexible Swept-Wing Jet Bomber. NACA RM L56E21a, 1956.

12. Nelson, Melvin A.: Wing Stress Analysis. [Model B-47B.] Vol. I.
Doc. No. D-10207 (Contract No. W33-038 ac-22413), Boeing Airplane
Co., Apr. 10, 1950.
13. Anon.: Weight and Balance Data. Model B-47A, Serial No. 49-1900,
Tech. Order No. AN-01-1B-40, 1950.

TABLE I-. FLIGHT CONDITIONS

Flight	Run	Mach number	Airplane weight, lb	Altitude, ft	Dynamic pressure, lb/sq ft	Center of gravity, percent M.A.C.	Fuel forward auxiliary tank, lb	Fuel forward main tank, lb	Fuel center auxiliary tank, lb	Fuel center main tank, lb	Fuel aft main tank, lb
4	19	0.70	108,900	25,000	265	20.97	0	7,700	0	12,500	7,200
4	20	.60	108,700	25,000	189	20.91	0	7,600	0	12,500	7,100
4	21	.51	108,400	25,000	128	20.85	0	7,500	0	12,400	7,000
6	12	.78	108,700	30,000	267	13.10	1,500	9,200	375	10,050	6,100
6	13	.74	108,400	30,000	244	13.12	1,500	9,000	375	10,050	6,000
6	14	.69	108,200	30,000	215	13.16	1,500	8,950	375	10,050	6,000
6	15	.64	107,600	30,000	187	13.03	1,500	8,700	375	10,050	5,800
10	3	.60	127,200	30,000	159	22.64	1,300	13,300	1,300	15,500	14,300
10	5	.68	126,300	30,000	200	22.39	1,300	13,100	1,300	15,100	14,000
10	6	.72	126,100	30,000	230	22.51	1,300	13,000	1,300	15,000	14,000
10	7	.76	125,400	30,000	255	22.96	1,300	12,600	1,300	14,700	14,000
10	9	.80	124,900	30,000	275	23.28	1,300	12,300	1,300	14,500	14,000

TABLE II.- EXPERIMENTAL FUSELAGE DEFLECTION COEFFICIENTS

(a) Deflection coefficients due to zero lift plus droop, $Z_0 + Z_i$

Flight	Run	Target		
		1	2	3
4	19	2.41	2.82	3.81
4	20	2.17	2.44	3.41
4	21	2.03	2.22	2.74
6	12	2.33	2.63	2.98
6	13	2.00	2.10	2.52
6	14	1.94	2.16	2.47
6	15	1.89	1.89	1.93
10	3	2.12	2.32	2.21
10	5	2.58	2.76	3.12
10	6	2.59	3.12	3.47
10	7	2.73	3.07	3.76
10	9	2.71	3.25	4.25

(b) Deflection coefficients due to normal-acceleration loads, Z_n

Flight	Run	Target		
		1	2	3
4	19	1.76	2.66	5.01
4	20	1.93	2.86	5.07
4	21	1.97	2.93	5.42
6	12	1.82	2.76	5.33
6	13	2.00	3.06	5.40
6	14	1.97	2.88	5.19
6	15	1.93	3.01	5.44
10	3	2.64	3.77	6.62
10	5	2.24	3.43	5.96
10	6	2.25	3.10	5.82
10	7	2.15	3.27	5.77
10	9	2.24	3.26	5.58

(c) Deflection coefficients due to pitching-acceleration loads, Z_q^*

Flight	Run	Target		
		1	2	3
4	19	0.83	1.85	5.38
4	20	1.40	2.73	6.14
4	21	1.58	2.52	6.24
6	12	1.14	2.07	4.78
6	13	1.80	2.82	5.48
6	14	1.65	2.79	5.34
6	15	1.23	3.22	5.44
10	3	3.12	4.30	9.52
10	5	2.00	3.69	7.84
10	6	1.71	2.38	7.40
10	7	1.39	2.69	7.48
10	9	1.54	2.85	6.37

(d) Deflection coefficients due to pitching-velocity loads, Z_q

Flight	Run	Target		
		1	2	3
4	19	-0.17	-0.84	-2.11
4	20	-.62	-1.26	-.67
4	21	-.20	-.47	-.33
6	12	-1.16	-.48	.72
6	13	-1.37	-2.12	-1.71
6	14	-.16	-.95	-.92
6	15	-1.17	-1.28	-1.82
10	3	-1.50	-1.96	-3.41
10	5	-.82	-1.32	-2.72
10	6	-.99	-.97	-3.00
10	7	-.83	-1.81	-2.75
10	9	-1.60	-1.94	-3.94

TABLE III.- TYPICAL TARGET DEFLECTIONS AND STANDARD ERRORS

[Flight 10, Run 7]

Target	Target-deflection coefficient and standard error for -				
	s_Z	$(Z_o + Z_i)$	Z_n	Z_d	Z_q
1	± 0.027	2.735 ± 0.037	2.153 ± 0.037	1.395 ± 0.169	-0.832 ± 0.249
2	± 0.022	3.077 ± 0.030	3.272 ± 0.030	2.696 ± 0.138	-1.818 ± 0.203
3	± 0.056	3.763 ± 0.076	5.778 ± 0.077	7.482 ± 0.351	-2.756 ± 0.518

TABLE IV.- COMPARISON OF SOME QUANTITIES OBTAINED IN THEORETICAL FUSELAGE

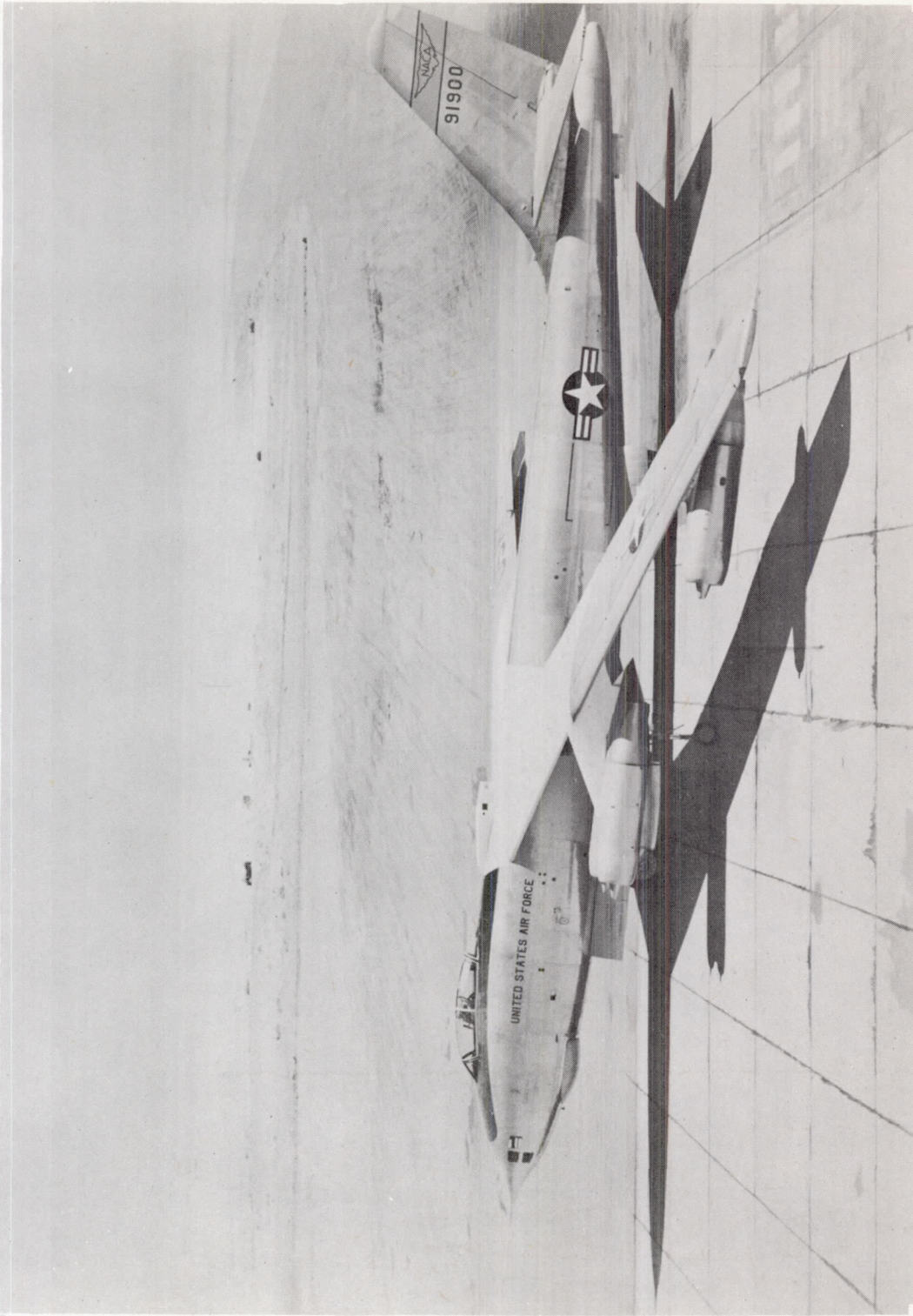
CALCULATIONS WITH EXPERIMENTAL RESULTS FROM SEVERAL SOURCES

Condition	Method	Weight, lb	Angle of attack, $d\alpha/dn$ (a)	Tail load, dL_t/dn (b)	Fuselage station of center of gravity	Wing root shear at $y = 54$ (c)	Pitch inertia I_y , lb-in.-sec (b)
Flight 4 Run 20	Experimental	108,700	0.083	902 (+ L_t up)	617.4	46,000	15,881,000
	Calculated	109,072	.084	1,372	613.4	49,000	14,659,749
Flight 10 Run 7	Experimental	125,400	.064	2,231	620.6	52,300	18,320,000
	Calculated	125,772	.067	2,916	617.2	55,800	17,734,298

(a) Experimental data from reference 5.

(b) Experimental data from preliminary results of strain-gage measurements on the wing and tail of the test airplane as obtained in the Langley Flight Research Division.

(c) Experimental data from preliminary results of strain-gage measurements on the wing and tail of the test airplane as obtained in the Langley Flight Research Division.



I-86692

Figure 1.- Photograph of test airplane.

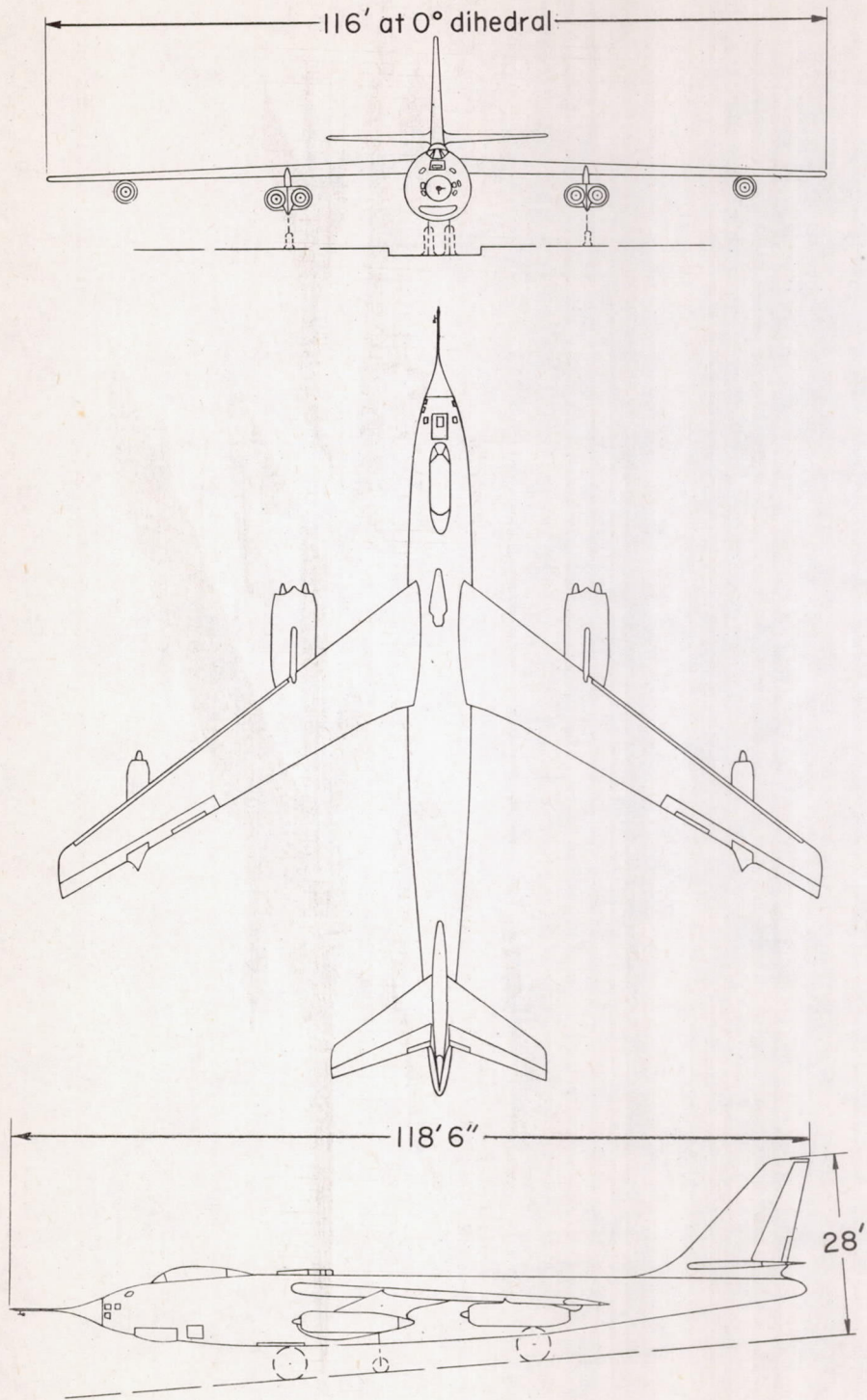
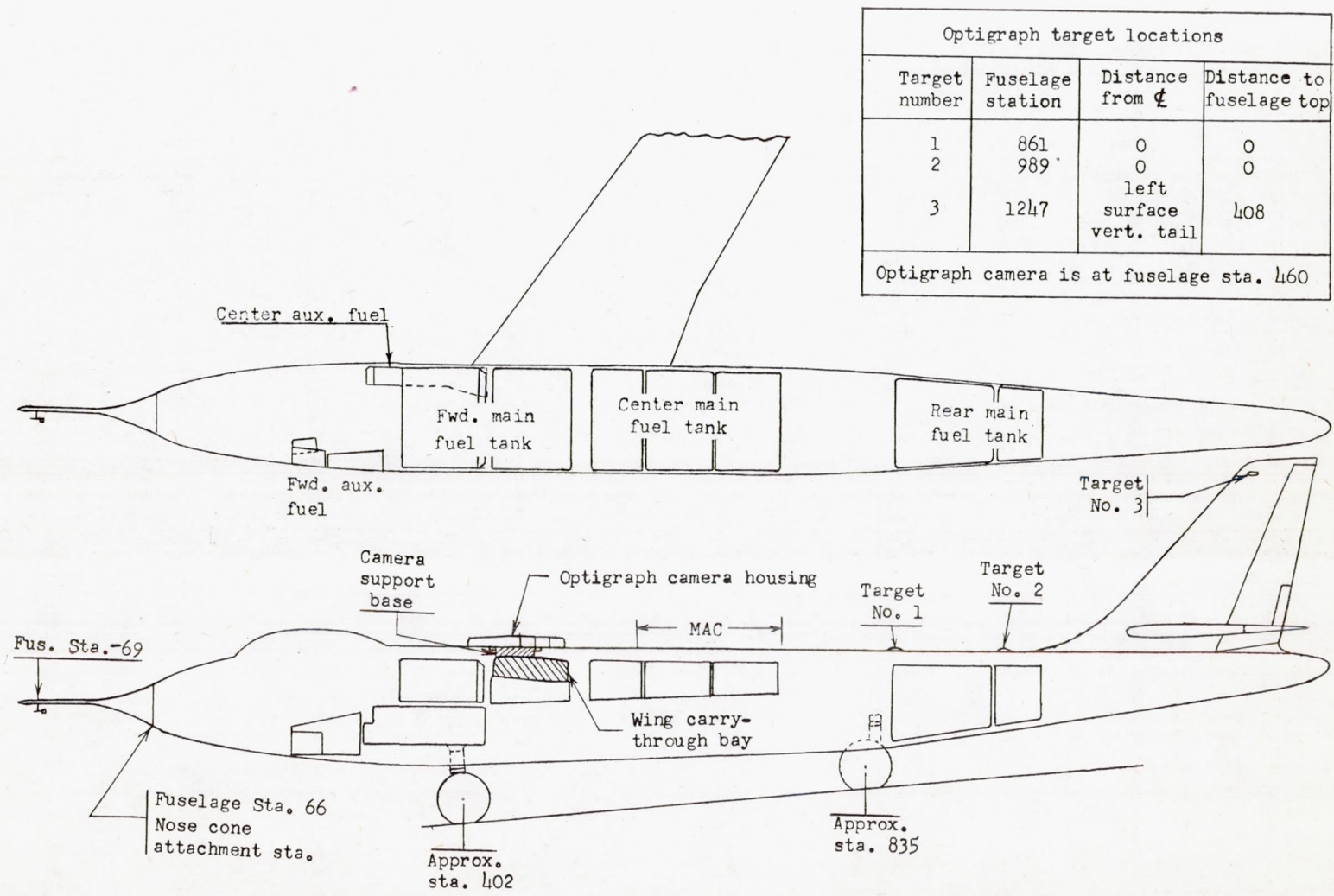


Figure 2.- Three views of test airplane.



Optigraph target locations			
Target number	Fuselage station	Distance from ϕ	Distance to fuselage top
1	861	0	0
2	989	0	0
3	1247	left surface vert. tail	408

Optigraph camera is at fuselage sta. 460

Figure 3.- Top and side view of test airplane showing optigraph camera and fuel-tank locations.

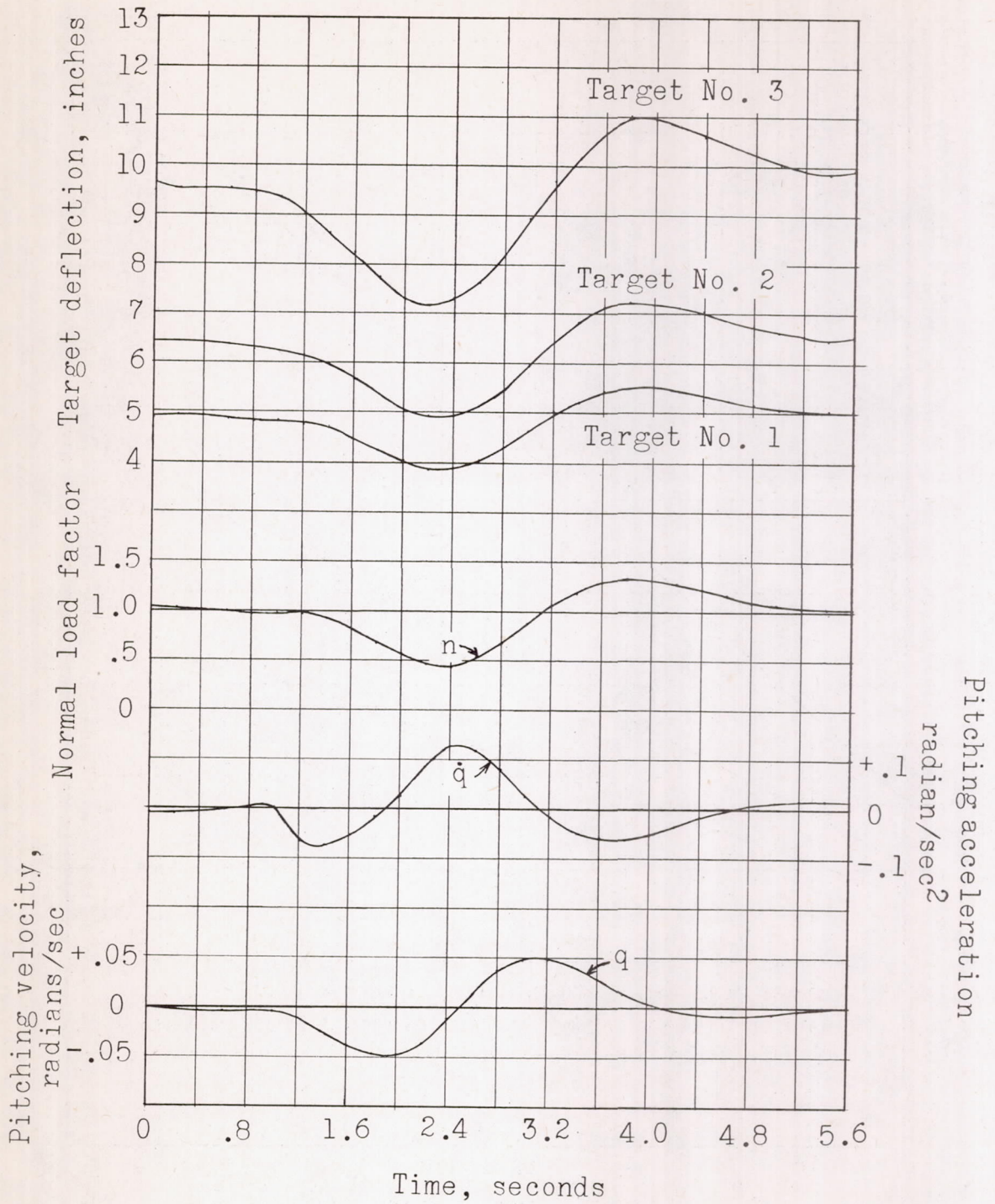


Figure 4.- Typical time history of fuselage deflections.

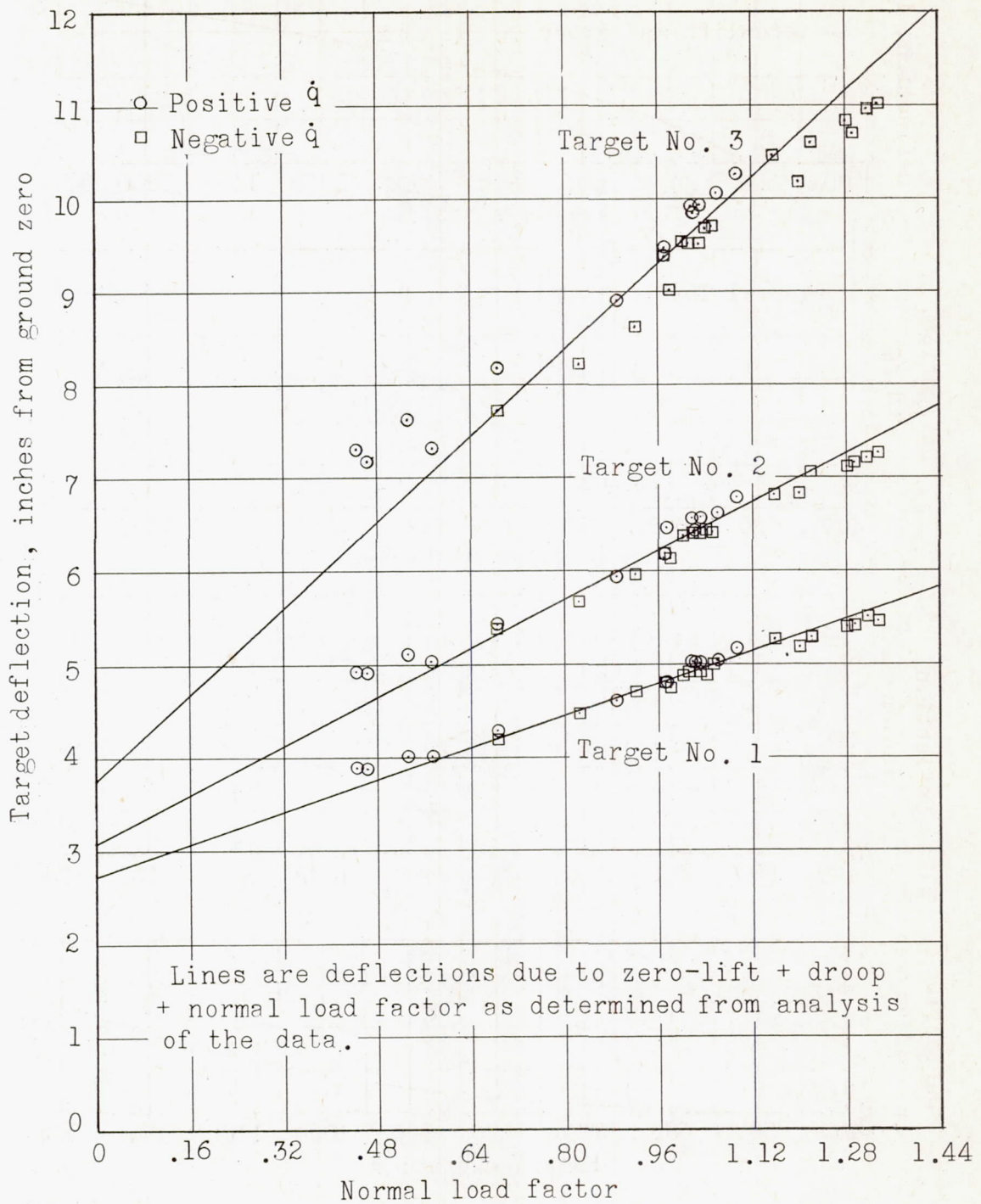


Figure 5.- Fuselage deflections measured at various load factors in a typical run.

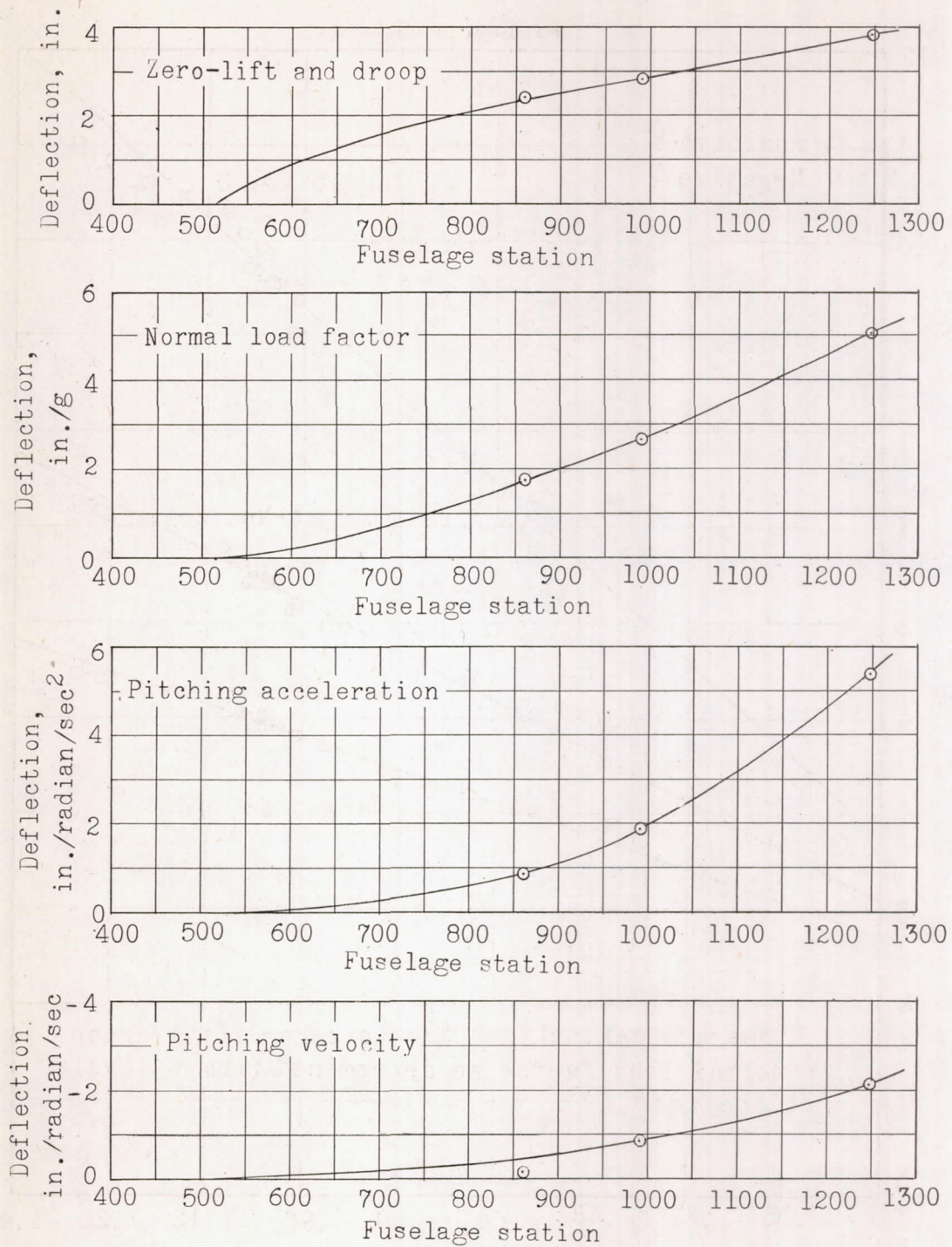


Figure 6.- Typical fuselage-deflection curves obtained from the deflection coefficients. $q^* = 265$ lb/sq ft; weight = 108,900 lb; $M = 0.70$.

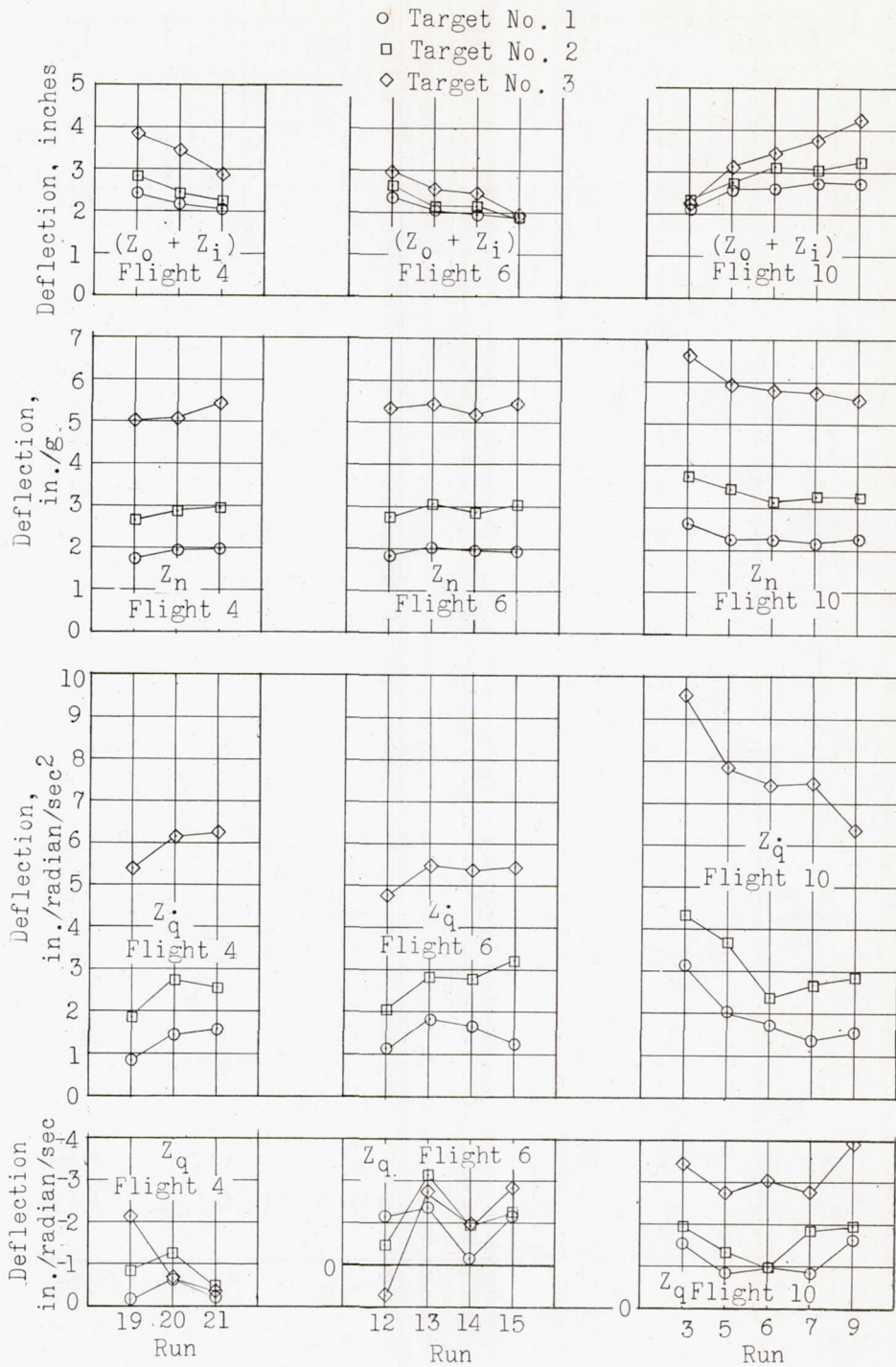


Figure 7.- Variations of the fuselage-deflection coefficients for the various runs.

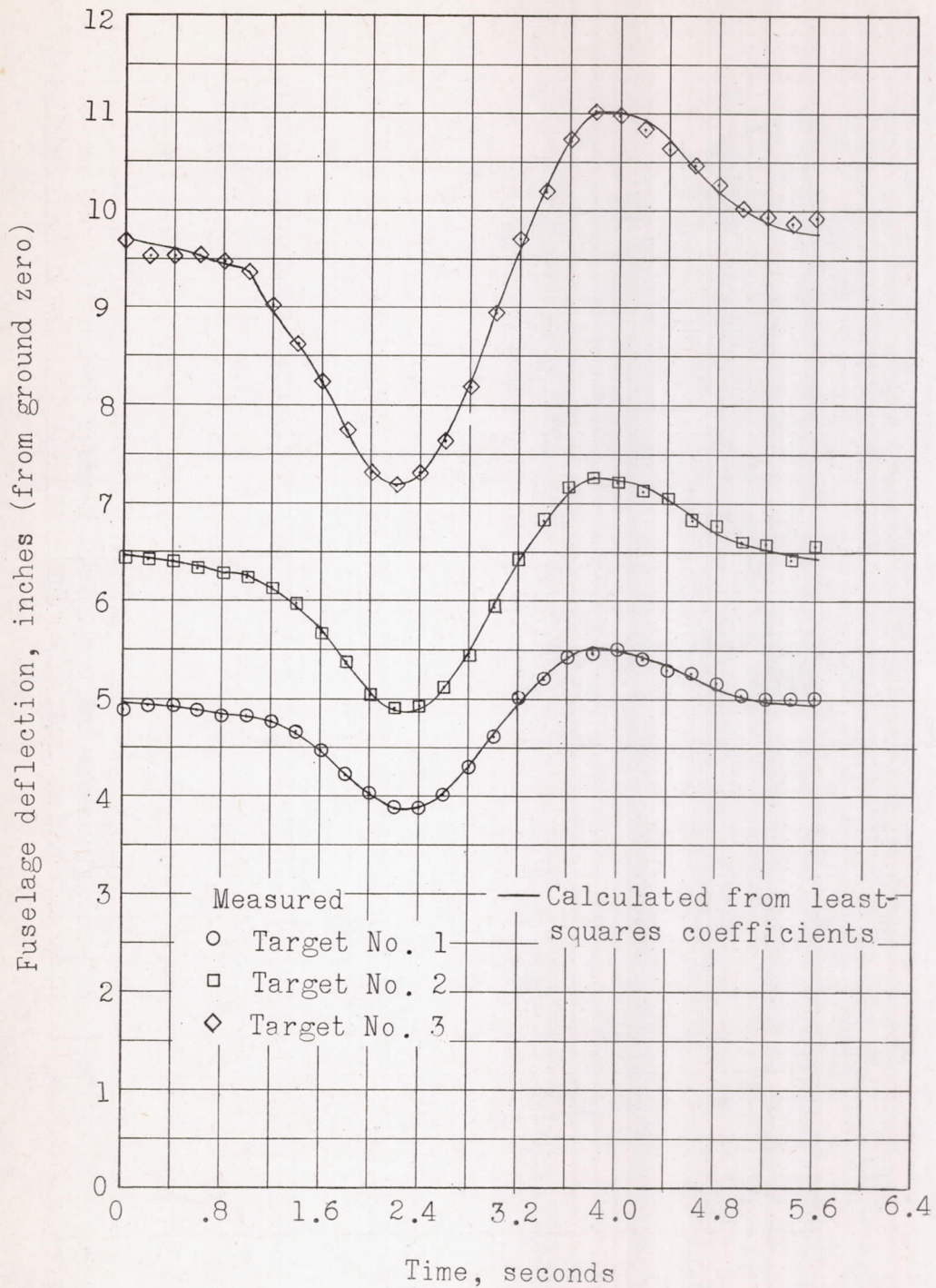


Figure 8.- Comparison of measured fuselage deflection with that calculated using the deflection coefficients.

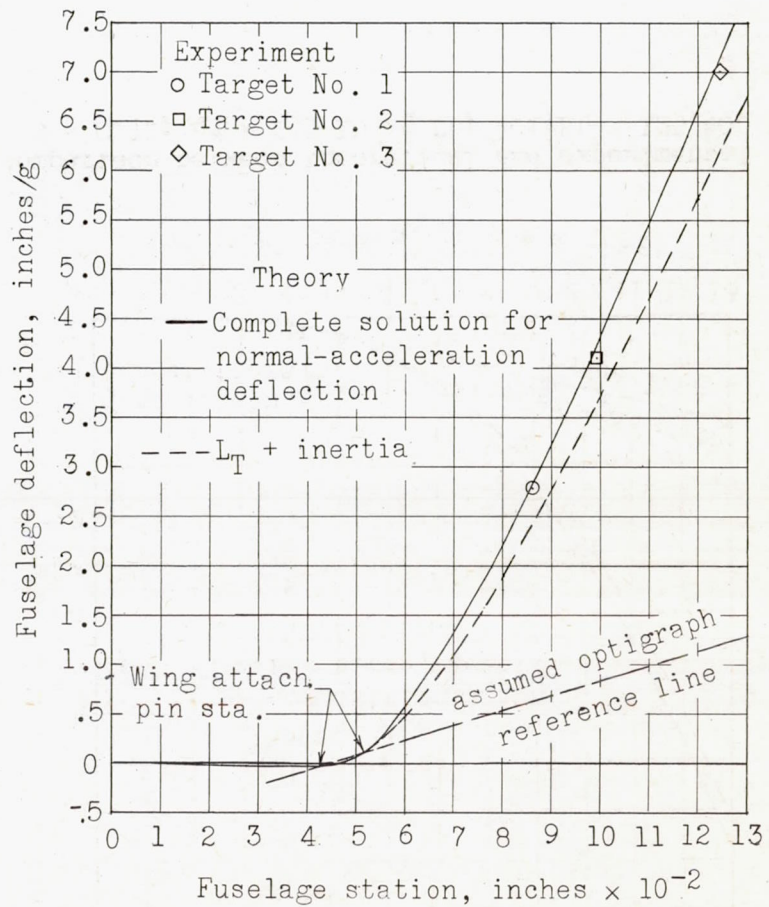
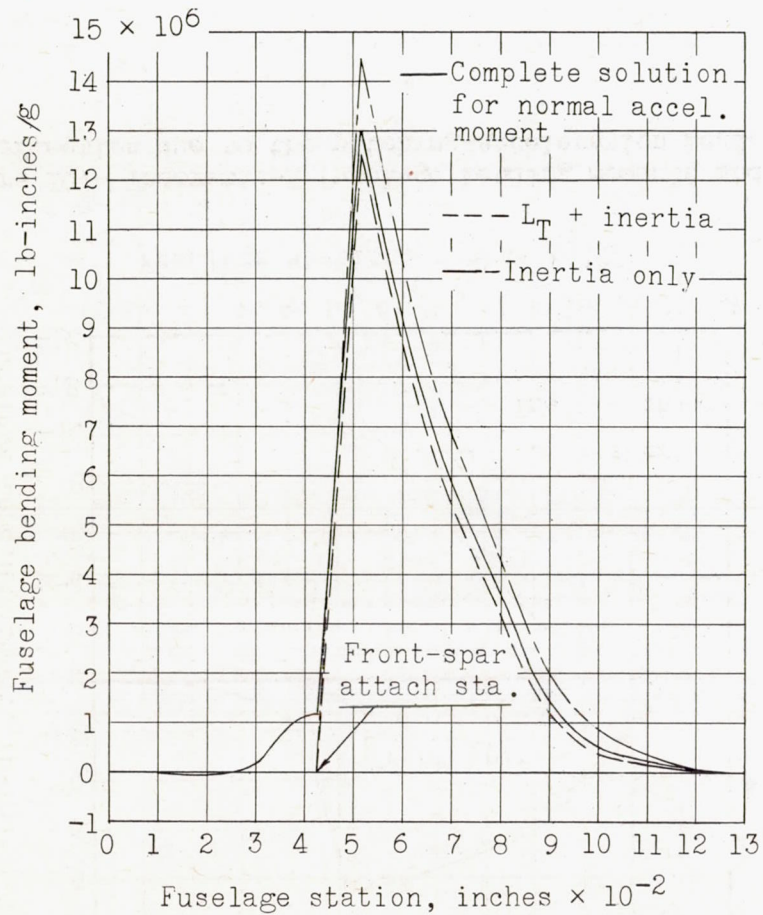


Figure 9.- Theoretical fuselage bending moments and comparison between theoretical and experimental deflections due to the normal-acceleration loads. Weight = 125,400 lb; $M = 0.76$; $q^* = 255$ lb/sq ft.

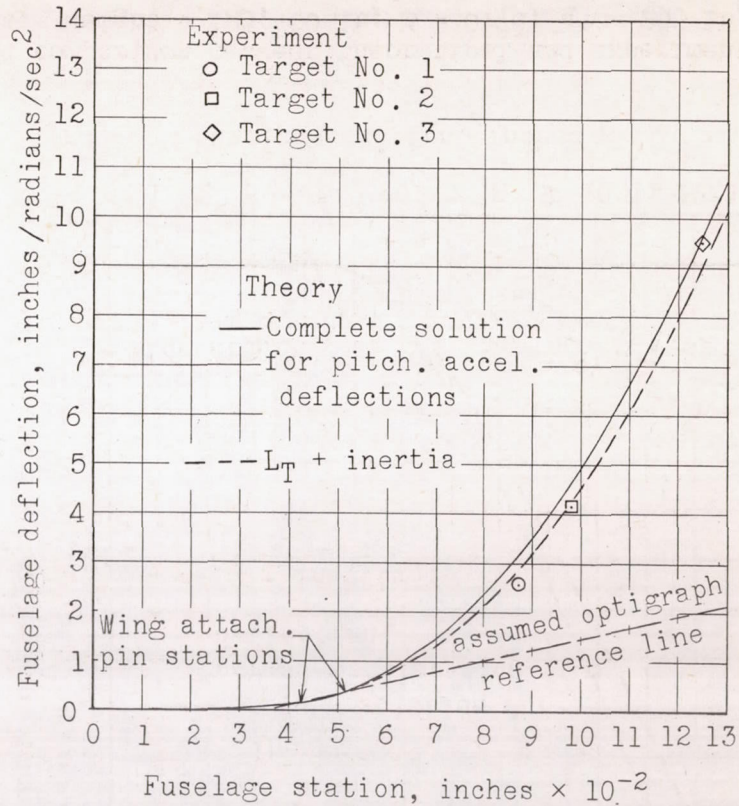
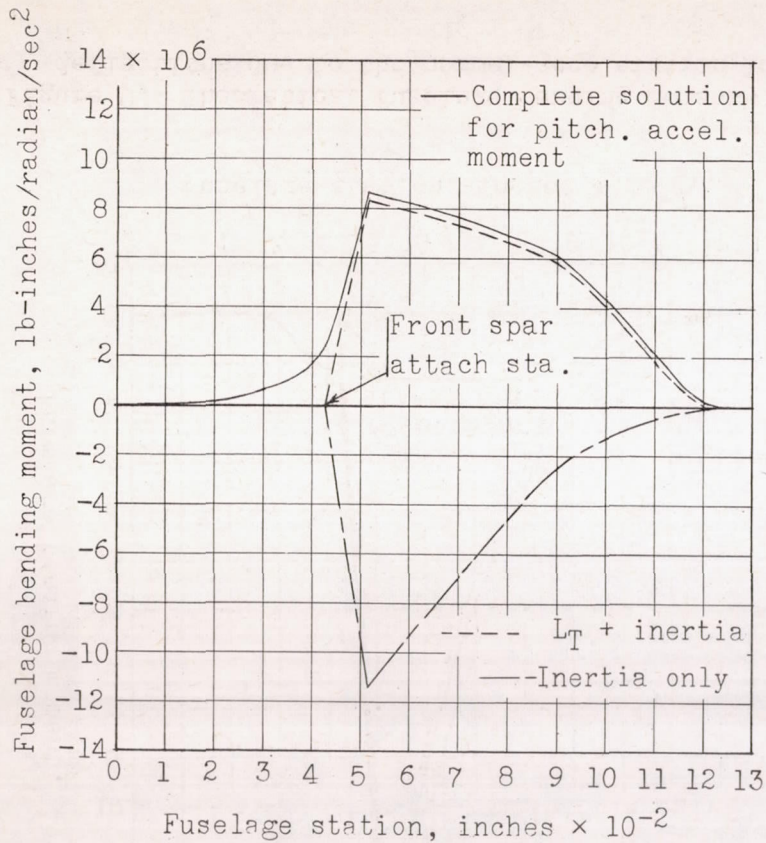


Figure 10.- Theoretical fuselage bending moments and comparison between theoretical and experimental deflection due to the pitching-acceleration loads. $M = 0.76$; $q^* = 255$ lb/sq ft; weight = 125,400 lb.

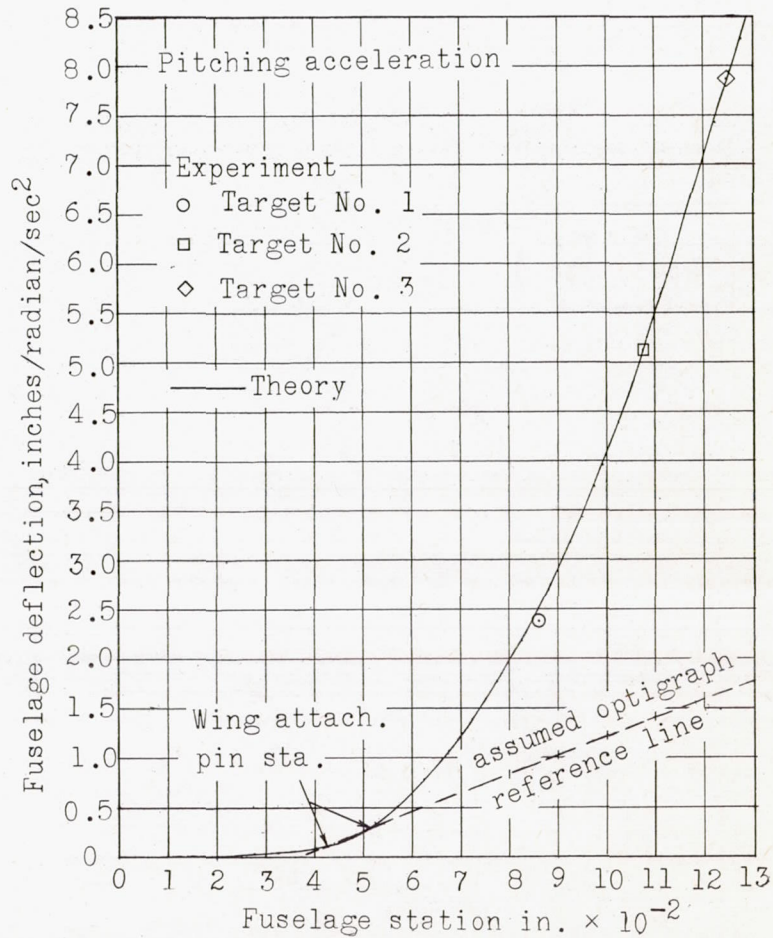
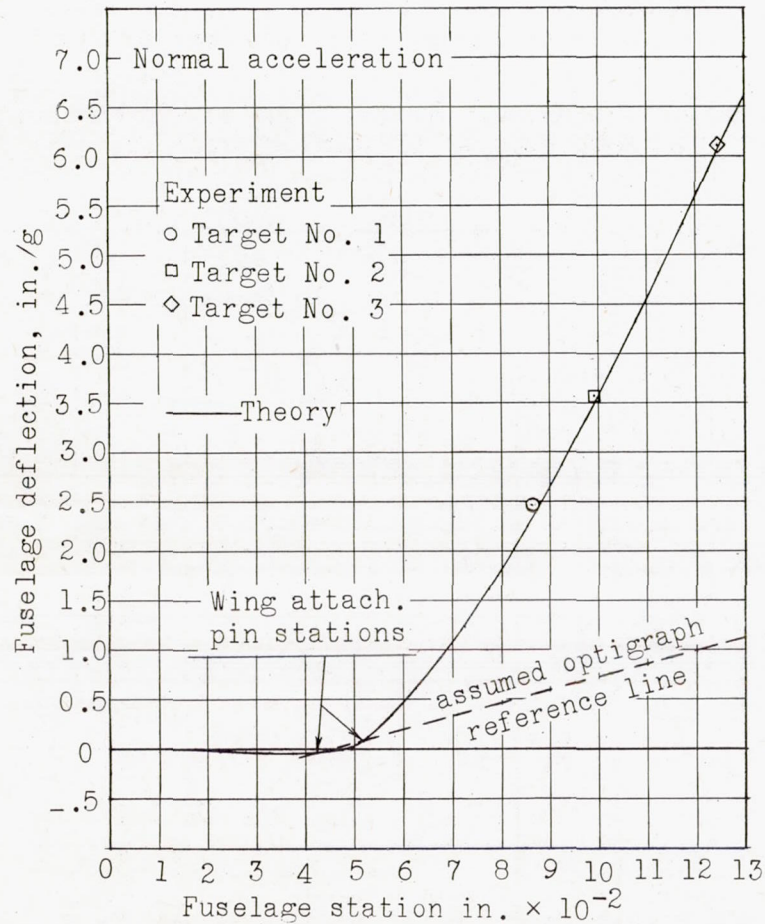


Figure 11.- Comparison of experimental and theoretical fuselage deflections due to the normal-acceleration and the pitching-acceleration loads. $M = 0.60$; weight = 108,700 lb; $q^* = 189$ lb/sq ft.

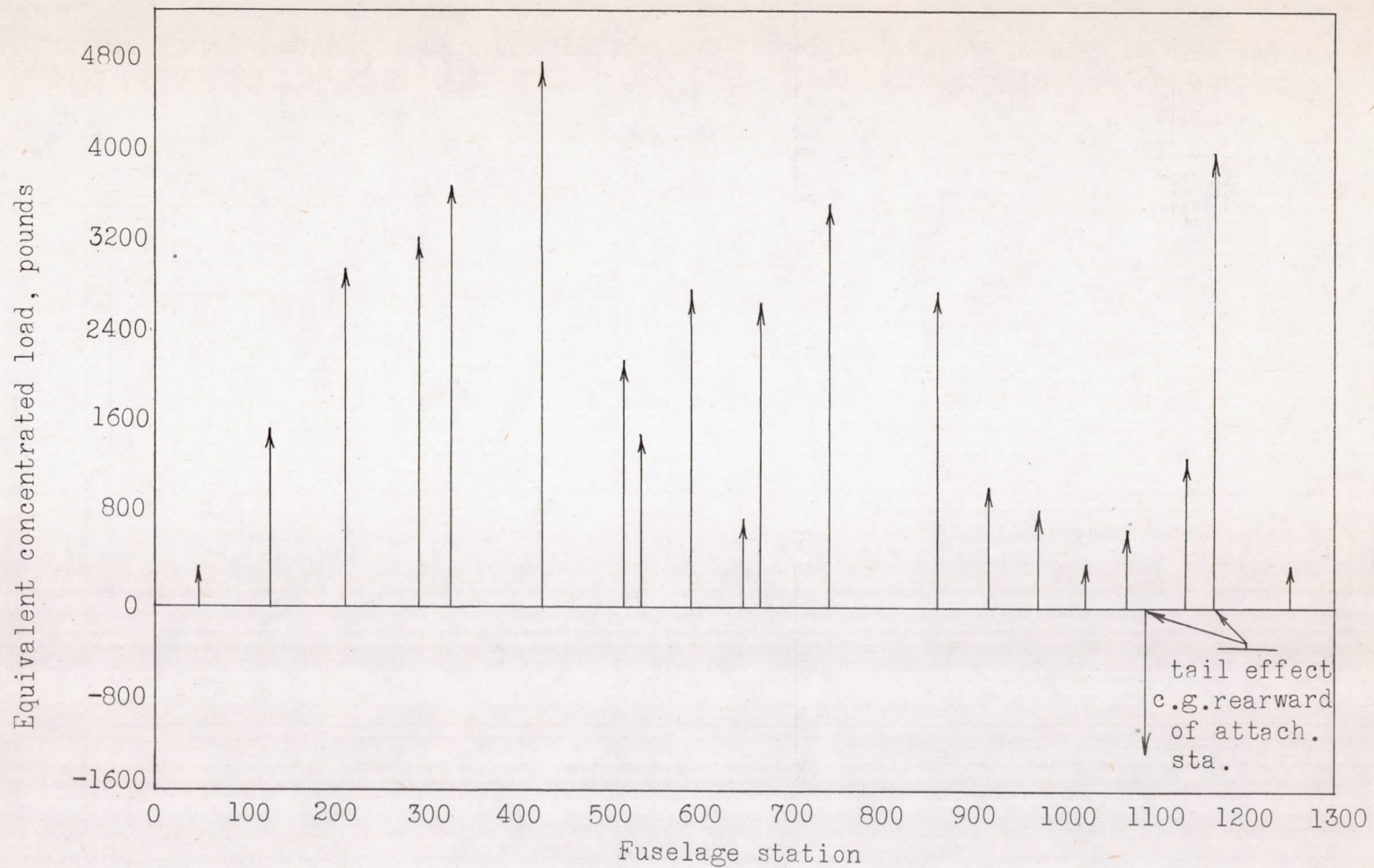


Figure 12.- Approximated weight distribution of the fuselage including weight of the pilots, instruments, and unavailable fuel.

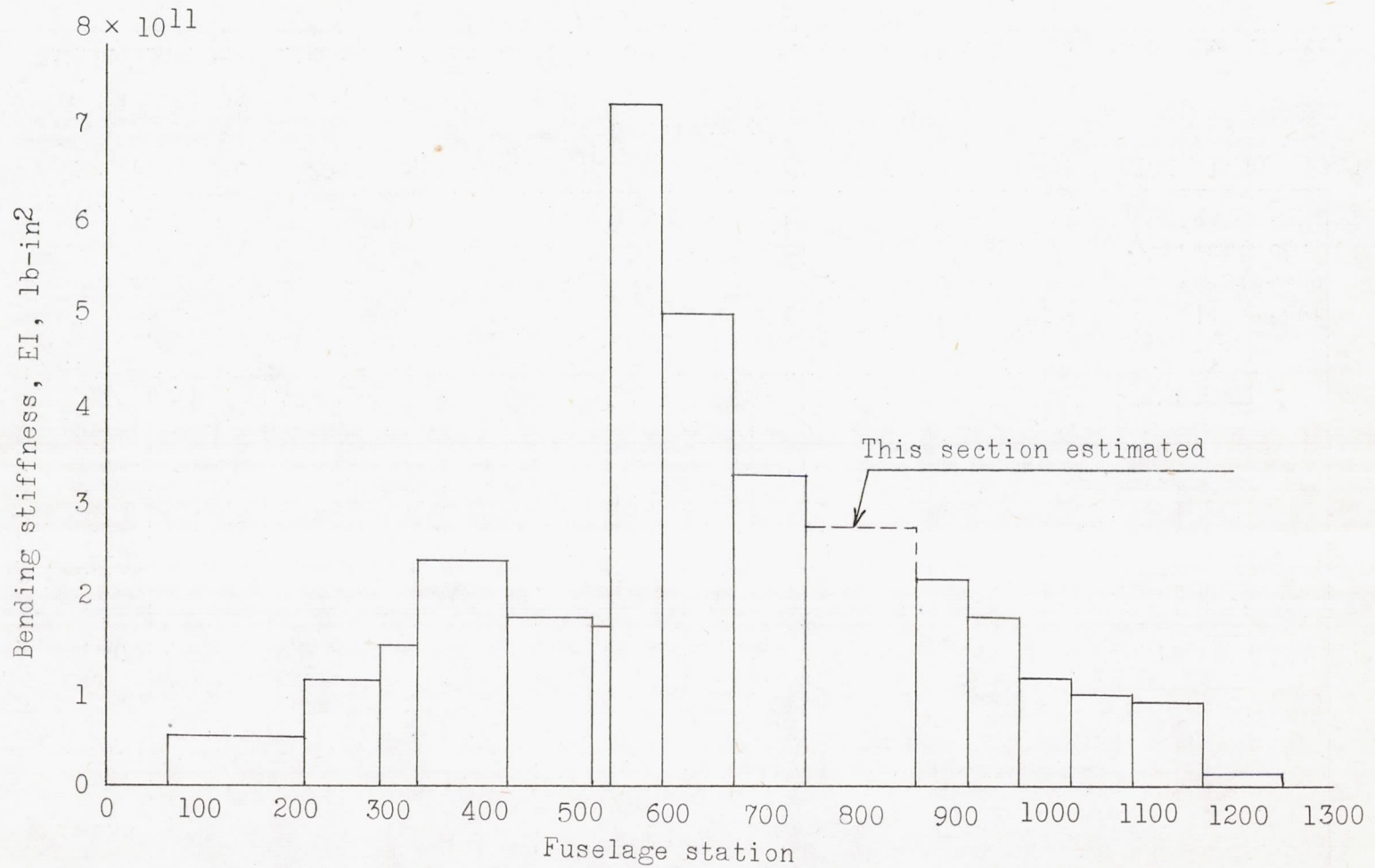


Figure 13.- Fuselage bending-stiffness distribution for positive bending (downward).

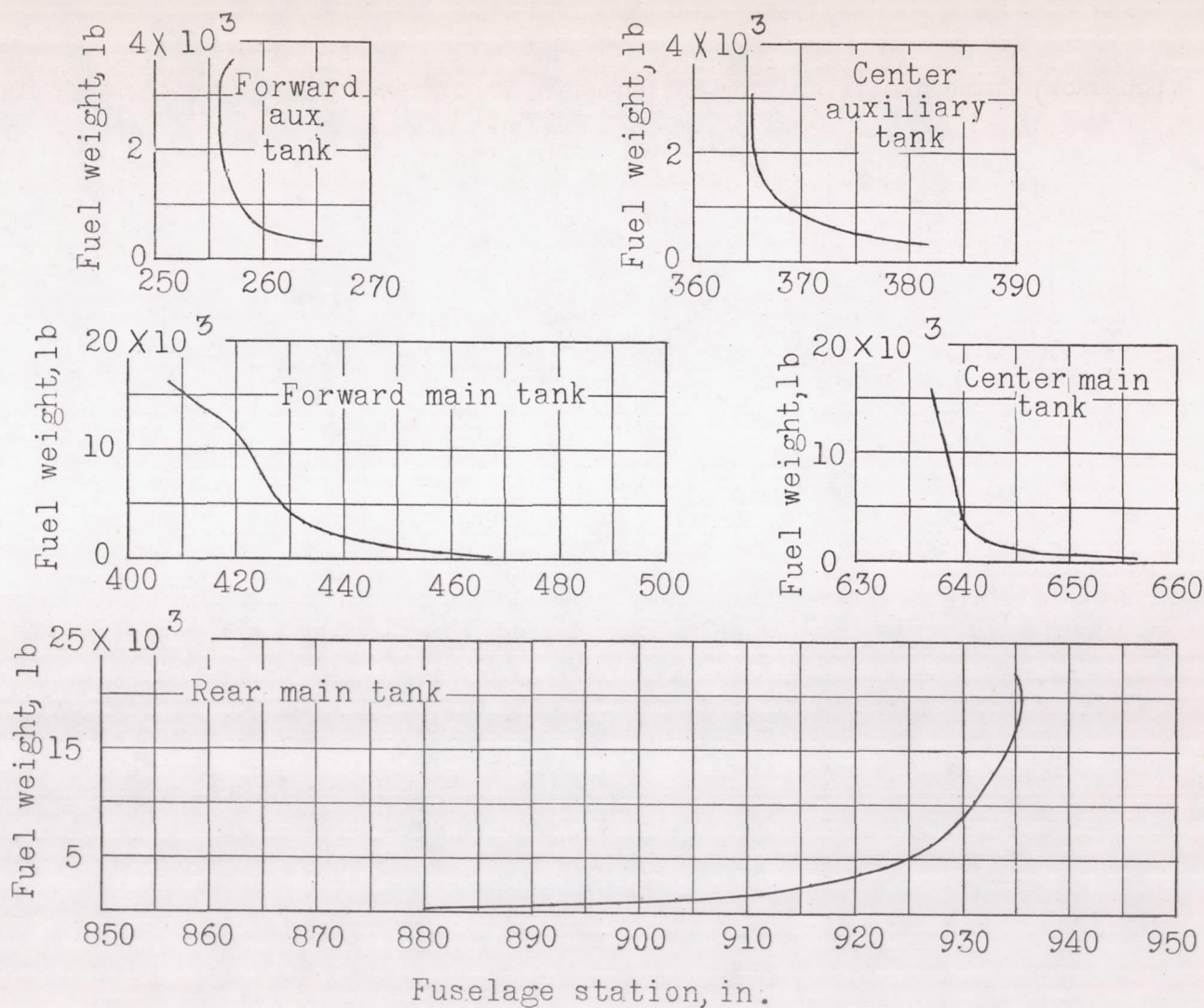


Figure 14.- Variation of fuel tank center of gravity with amount of fuel (data from ref. 12).